A bacterial GW-effector targets Arabidopsis AGO1 to promote pathogenicity and induces Effector-triggered immunity by disrupting AGO1 homeostasis

Odon Thiébeauld[1], Magali Charvin[1§], Meenu Singla Rastogi[1§], Fan Yang[2,3], Dominique Pontier[4], Cécile Pouzet[5], Laure Bapaume[1], Guangyong Li[2,3], Laurent Deslandes[6], Thierry Lagrange[4], James R. Alfano[2,3], and Lionel Navarro[1*]

[1] Institut de Biologie de l'Ecole Normale Supérieure (IBENS), Ecole normale supérieure, CNRS, INSERM, PSL Research University, 75005 Paris, France

[2] Department of Plant Pathology, University of Nebraska, Lincoln, NE 68588-0722, USA

[3] Center for Plant Science Innovation, University of Nebraska, Lincoln, NE 68588-0660, USA

[4] Laboratoire Génome et Développement des Plantes, CNRS/Université de Perpignan via Domitia, UMR5096, 66860 Perpignan, France

[5] Plateforme Imagerie-Microscopie, Fédération de Recherche FR3450, CNRS, Castanet-Tolosan, France

[6] LIPM, Université de Toulouse, INRA, CNRS, Castanet-Tolosan, France

§ These authors contributed equally to the work

* correspondence: lionel.navarro@ens.fr (L.N.)

Running title: A BSR suppresses AGO1 activity and triggers ETI

SUMMARY

Pseudomonas syringae **type-III effectors were previously found to suppress the Arabidopsis miRNA pathway through elusive mechanisms. Here, we first show that HopT1-1 effector promotes pathogenicity by suppressing the Arabidopsis AGO1-dependent microRNA (miRNA) pathway. We further demonstrate that HopT1-1 interacts with, and suppresses the activity of, AGO1 through conserved glycine/tryptophan-(GW) motifs. HopT1-1 dampens PAMP-Triggered-Immunity (PTI) in a GW-dependent manner and its presence mimics the impaired PTI responses, which were also observed in *ago1* mutants. In addition, the silencing suppression activity of HopT1-1 induces Effector-Triggered-Immunity (ETI), which is correlated with an over-accumulation of silencing factors that are controlled by miRNAs, including AGO1. Remarkably, alleviating miR168-directed silencing of *AGO1* was sufficient to trigger an ETI-like response, orchestrated by typical disease resistance-immune signaling factors, suggesting that HopT1-1-induced perturbation of AGO1 homeostasis is a trigger of ETI activation. In summary, this study reports for the first time a strategy used by a bacterial effector to directly target an AGO protein and on how plants perceive its silencing suppression activity to trigger a host counter-counter defense.**

INTRODUCTION

Plants and animals have evolved sophisticated inducible immune responses to defend themselves against pathogens. The first layer of the plant immune system relies on the recognition of Pathogen- or Microbe-Associated Molecular Patterns (PAMPs or MAMPs) that are sensed by surface-localized Pattern-Recognition

Receptors (PRRs) (Couto and Zipfel., 2016). Classical plant PRRs are composed of receptor-like kinases (RLKs) and receptor-like proteins (RLPs) that are structurally and functionally analogous to animal Toll-Like Receptors (TLRs) (Li *et al*., 2016). The most characterized plant PRRs are the leucine-rich repeat receptor-like kinases FLS2 and EFR, which recognize conserved epitopes from bacterial flagellin or elongation factor Tu, respectively (Gómez-Gómez and Boller, 2000; Zipfel *et al*., 2006). Upon ligand binding, these receptors initiate a complex phosphorylation cascade at the PRR complex that leads to early signaling events, which include production of reactive oxygen species (ROS), activation of mitogen-activated-protein-kinases (MAPKs) and differential expression of thousands of genes (Gómez-Gómez *et al*. 1999; Felix and Boller, 1999; Zipfel *et al*., 2004; Navarro *et al*., 2004; Zipfel *et al*., 2006; Couto and Zipfel, 2016). Later responses involve biosynthesis of the phytohormone salicylic acid (SA) and cell wall modifications such as callose deposition, which ultimately culminate in PAMP-triggered immunity (PTI) (Hauck *et al*., 2003; Tsuda and Katagiri, 2010). Pathogens secrete virulence determinants, referred to as pathogen effectors, which can suppress PTI to cause disease (Jones and Dangl, 2006). As a counter-counter defense mechanism, plants have evolved disease resistance (R) proteins that can recognize the presence of pathogen effectors. Most R proteins belongs to the nucleotide-binding domain (NBD), leucine-rich repeat (NLR) superfamily, which are also present in animals (Jones *et al*., 2016). Some plant NLRs recognize pathogen effectors indirectly by sensing their effects on host targets that are indispensable for the virulence function of these effectors, as postulated by the Guard Model (Van der Biezen and Jones, 1998; Dangl and Jones, 2001). This model notably provides some explanation for why multiple pathogen effectors, produced by unrelated pathogens, could be perceived by a limited number

of NLRs that guard the integrity of critical host immune factors (guardees). After sensing pathogen effectors, plant NLRs induce Effector-triggered immunity (ETI), a potent immune response that significantly overlaps with PTI, although with a stronger amplitude (Tsuda and Katagiri, 2010; Navarro *et al*., 2004). ETI generally culminates into pronounced SA production, which is often accompanied by a form of host programmed cell death referred to as the hypersensitive response (HR) (Dangl and Jones, 2001). Recently, several endogenous short interfering RNA (siRNAs) and microRNAs (miRNAs) were found to fine-tune PTI and ETI responses (Staiger *et al*., 2013; Pumplin and Voinnet, 2013), implying a key role of Post-Transcriptional Gene Silencing (PTGS) in the regulation of the plant immune system.

PTGS is an ancestral post-transcriptional gene regulatory process. The core mechanism of PTGS involves the production of double-stranded RNA (dsRNA) precursors, which are processed by DICER-LIKE (DCL) ribonucleases into 20-24 bp small RNA duplexes (Bologna and Voinnet., 2014). These small RNA duplexes associate with an Argonaute (AGO) protein, the central component of a multiprotein RNA-induced silencing complex (RISC) (Vaucheret, 2008). The guide small RNA further directs AGO-RISC onto sequence complementary mRNA targets to trigger their post-transcriptional silencing. In plants, this phenomenon is manifested by endonucleolytic cleavage (so-called 'slicing') and/or translational inhibition of small RNA targets (Llave *et al*., 2002; Rhoades *et al*., 2002; Palatnik *et al*., 2003; Brodersen *et al*., 2008; Chen, 2004; Poulsen *et al*., 2013). *Arabidopsis thaliana* encodes 4 DCLs and 10 AGOs. DCL1 processes miRNA precursors with the help of other factors including the zinc-finger domain-containing protein SERRATE (SE) (Park *et al*., 2002; Finnegan *et al*., 2003; Kurihara and Watanabe, 2004; Lobbes *et al*., 2006). This reaction yields miRNA/miRNA* duplexes, where miRNA is the guide

strand and miRNA* the passenger strand. DCL2, DCL3 and DCL4 process endogenous and viral-derived dsRNAs into siRNA duplexes (Bologna and Voinnet, 2014). AGO1 is a major PTGS effector, which is loaded with miRNAs and siRNAs and plays an important role in antiviral defense and in bacterial PAMP-induced gene induction and callose deposition (Vaucheret, 2008; Morel *et al*., 2002; Li *et al*., 2010). AGO2 not only plays a critical role in antiviral silencing but is also required for antibacterial resistance mediated by the disease resistance protein RPS2 (Carbonell *et al*., 2010; Harvey *et al*., 2011; Jaubert *et al*., 2011; Zhang *et al*., 2011). AGO4 has also been reported to contribute to antiviral silencing and to antibacterial basal resistance (Agorio and Vera, 2007; Brosseau *et al*., 2016).

Small non-coding RNAs have been implicated in various biological processes and play a key role in controlling plant-pathogen interactions. In the context of plant-viral interactions, viral-derived siRNAs repress translation, replication or accumulation of viral RNA, thereby inhibiting viral replication (Hamilton and Baulcombe., 1999; Pumplin and Voinnet., 2013; Baulcombe, 2015). In addition, plant miRNAs and siRNAs can modulate resistance against bacterial, fungal and oomycete phytopathogens by targeting either positive or negative regulators of PTI and/or ETI (Weiber *et al*., 2015). This phenomenon has been well characterized in the context of plant-bacterial interactions. As examples, miR393, miR160 and miR167 are PAMP-induced miRNAs that are loaded into Arabidopsis AGO1 to negatively regulate auxin signaling during PTI (Navarro *et al.*, 2006; Fahlgren *et al*., 2007; Li *et al.*, 2010), while miR393b* is strongly enriched in Arabidopsis AGO2 during ETI and targets a negative regulator of defense that acts downstream of the disease resistance protein RPS2 (Zhang *et al.*, 2011). Furthermore, several endogenous siRNAs were found to

be induced in response to a *Pseudomonas syringae* strain carrying AvrRpt2 and specifically required for *RPS2*-mediated resistance (Katiyar-Agarwal *et al*., 2006; Katiyar-Agarwal *et al*., 2007). There is also growing evidence that filamentous phytopathogens differentially regulate functionally relevant endogenous small RNAs. For example, soybean miR393 is induced in response to *Phytophthora sojae* and positively regulates resistance against this oomycete pathogen (Wong *et al*., 2014).

Given that small non-coding RNAs play a major role in regulating plant immune responses as well as in targeting viral transcripts, it is not surprising that many pathogens have evolved PTGS suppression mechanisms to cause disease. This phenomenon has been extensively characterized in plant-viral interactions and we know now that most, if not all, plant RNA viruses encode Viral Suppressors of RNA silencing (VSRs) (Pumplin and Voinnet, 2013). These proteins suppress different steps of PTGS and AGO1 has emerged as a critical VSR target (Zhang *et al* 2006; Derrien *et al*., 2012; Azevedo *et al*., 2010; Giner *et al*., 2010). Interestingly, RNA silencing suppressors were also reported from oomycete and bacterial phytopathogens (Navarro *et al*., 2008; Qiao *et al*., 2015). In particular, we found that growth of a type-III secretion defective mutant of *P. syringae* pv. *tomato* strain DC3000 (*Pto* DC3000) and of non-adapted bacteria was significantly enhanced in Arabidopsis mutants that are impaired in miRNA biogenesis (Navarro *et al*., 2008). These results provide evidence that the Arabidopsis miRNA pathway is essential for antibacterial basal immunity and suggest that *Pto* DC3000 effectors must have evolved to suppress this small RNA pathway to cause disease. Accordingly, we have identified a series of Bacterial Suppressors of RNA silencing (BSRs) from this bacterium that inhibit all the steps of the Arabidopsis miRNA pathway (Navarro *et al*.,

2008). However, it remains unknown whether such BSRs could directly interact with components of the RNA silencing machinery to suppress miRNA activity and if Arabidopsis could have evolved strategies to detect the presence of these bacterial effectors.

Here, we found that the *Pto* DC3000 type-III secreted Hrp outer protein T1-1 (HopT1-1) is a critical virulence determinant of *Pto* DC3000 that promotes pathogenicity by suppressing the AGO1-dependent miRNA pathway in Arabidopsis. We showed that HopT1-1 can physically interact with Arabidopsis AGO1, at least in part, through two conserved GW motifs, which represent AGO-binding platforms previously found in some metazoan and plant silencing factors (Till *et al*., 2007; El-Shami *et al*., 2007; Azevedo *et al*., 2011). We also provided evidence that the GW motifs of HopT1-1 are essential for its ability to suppress not only miRNA activity but also PTI responses (PAMP-triggered ROS production and callose deposition). These results indicate that silencing suppression activity of HopT1-1 is coupled with its virulence function and likely relies on the targeting of Arabidopsis AGO1, which was found to be essential for PAMP-induced ROS production and callose deposition. Furthermore, we observed that constitutive expression of HopT1-1 in Arabidopsis triggers a potent autoimmune response that is dependent on classical NLR-immune signaling factors. Importantly, this phenotype is directed by the BSR activity of HopT1-1 and is correlated with an enhanced accumulation of silencing factors that are controlled by miRNAs, including AGO1. Remarkably, alleviating the miR168-directed control of AGO1 in Arabidopsis is sufficient to trigger an autoimmune phenotype that is also dependent on typical NLR-immune signaling factors. These findings indicate that HopT1-1-induced disruption of AGO1 homeostasis is likely a trigger of ETI activation.

RESULTS

HopT1-1 is a key pathogenicity determinant that promotes growth of *Pto* DC3000 by suppressing the Arabidopsis AGO1-dependent miRNA pathway

HopT1-1 is an experimentally validated type-III secreted protein expressed from the pDC3000A plasmid of *Pto* DC3000 (Guo *et al*., 2005). Although HopT1-1 was previously shown to suppress the transcriptional activation of a PAMP-responsive gene (Li *et al*., 2005), there is no experimental evidence indicating a role for this effector in promoting bacterial multiplication *in planta*. To test this possibility, we first generated a *Pto* DC3000 mutant strain deleted of *hopT1-1*, hereafter referred to as *Pto* Δ*hopT1-1*, and assessed the ability of this strain to multiply in leaves of the Arabidopsis Col-0 accession. Upon dip-inoculation of wild type (WT) plants, we found that the *Pto* Δ*hopT1-1* mutant strain exhibited at least ~ 10 times lower bacterial titer at 3 days post-inoculation (dpi) compared to wild type *Pto* DC3000 (Figures 1 and S1). This result indicates that HopT1-1 is a functionally relevant effector of *Pto* DC3000 that contributes to bacterial growth *in planta*.

HopT1-1 was previously shown to suppress AGO1-mediated miRNA- and siRNA-functions (Navarro *et al*., 2008), but the relevance of this interference in bacterial pathogenesis remains unknown. We took advantage of the *Pto* Δ*hopT1-1* mutant strain and examined whether its growth defect could be potentially rescued in *ago1* mutants. For this purpose, we dip-inoculated the *Pto* Δ*hopT1-1* strain on WT plants and on three different weak alleles of *AGO1*, namely *ago1-25*, *ago1-26* and *ago1-27* (Morel *et al*., 2002), and subsequently monitored bacterial titers at 3 dpi. We also included in this assay the *ago2-1*, *ago4-2* and *ago4-3* mutants, as *AGO2* and *AGO4*

were previously characterized in *RPS2*-mediated resistance and in antibacterial basal resistance, respectively (Zhang *et al*., 2011; Agorio and Vera, 2007). Strikingly, the growth defect of *Pto* Δ*hopT1-1* was fully rescued in all *ago1* allelic mutants (Figures 1A, S1A and S1B), while it remained unaltered in *ago2* and *ago4* mutants (Figures 1B and S1C). To further test if the phenotype observed in *ago1* mutants was specific to the *Pto* Δ*hopT1-1* mutant strain, and not due to collateral effects caused by *ago1* developmental phenotypes, we repeated this assay with a *Pto* DC3000 mutant deleted of *hopC1* (*Pto* Δ*hopC1*). The latter effector partially contributes to *Pto* DC3000 multiplication in Arabidopsis WT leaves but does not interfere with miRNA action (Figures 1A/C, S1A and S1D; Navarro *et al*., 2008). Importantly, the partial *Pto* Δ*hopC1* growth defect observed in WT plants was not rescued in *ago1-27* plants (Figures 1A and S1A), indicating that the restoration of bacterial growth detected in *ago1* mutants was specific to the *Pto* Δ*hopT1-1* strain. Collectively, these results provide evidence that *AGO1* is a major genetic target of HopT1-1 and that AGO1 function must be impaired by HopT1-1 to promote growth of *Pto* DC3000 *in planta*.

Given that AGO1 is required for both miRNA- and siRNA-functions, we next wanted to assess which of the two activities could be genetically targeted by HopT1-1 to promote growth of *Pto* DC3000 *in planta.* We first tested if the *Pto* Δ*hopT1-1* growth defect could be rescued in *dcl1-11* and *se-1* mutants, which are both specifically impaired in miRNA biogenesis (Lobbes *et al*., 2006; Zhang *et al*. 2008). Similar to the observation made in *ago1* alleles, the *Pto* Δ*hopT1-1* growth defect was fully rescued in these mutants (Figures 1C, S1D and S1E). Furthermore, the *Pto* Δ*hopT1-1* growth rescue phenotype observed in *se-1* mutant was also specific to this strain as it did not occur with the *Pto* Δ*hopC1* mutant strain (Figures 1C and S1D). We next repeated the same assay in *suppressor of gene silencing 3* (*sgs3-1*), *RNA-*

dependent RNA-Polymerase 1 (*rdr1-1) rdr2-1 rdr6-15* and *dcl2-1 dcl4-2* mutants, which are impaired in the biogenesis of endogenous siRNAs and viral-derived siRNAs (Mourrain *et al*., 2000; Dalmay *et al*., 2000; Xie *et al*., 2004; Deleris *et al*., 2006; Diaz-Pendon *et al*., 2007; Donaire *et al*., 2008). Interestingly, we did not find any growth restoration of the *Pto* Δ*hopT1-1* strain in these siRNA-defective mutants (Figures 1D, S1F and S1G). Altogether, these results indicate that HopT1-1-triggered suppression of AGO1-mediated miRNA function, but not of AGO1-mediated siRNA function, is critical to promote growth of *Pto* DC3000 *in planta*.

HopT1-1 physically interacts with Arabidopsis AGO1, at least in part, through two conserved GW motifs

The above genetic data suggested that HopT1-1 could interact with Arabidopsis AGO1 to alter its function. The AGO-binding function of GW/WG platforms, present in some endogenous silencing factors as well as in some VSRs (Azevedo *et al*., 2011; Azevedo *et al*., 2010; Karran and Sansfaçon, 2014; Aqil *et al*., 2013; Giner *et al*., 2010), prompted us to examine the protein sequence of HopT1-1 for the presence of such motifs. We found that there are three GW repeats at positions 80, 113 and 182, which are referred to here as GW1, GW2 and GW3, respectively (Figure 2A). These GW motifs are conserved in a putative HopT1-1 ortholog derived from the phylogenetically divergent marine bacterium *Marinomonas mediterranea* (Figure S2A), suggesting that they might be functionally relevant. To test this idea experimentally, we generated tryptophan to phenylalanine substitutions (GW>GF) in each tryptophan residue of the GW motifs (Figure 2A). It is noteworthy that these point mutations do not alter the stability of HopT1-1 when expressed in *Nicotiana benthamiana* or Arabidopsis plants (Figures S3A, S3B and S4A). We further

analyzed the ability of HopT1-1 WT and of the triple GW>GF mutant version referred to as HopT1-1m3 to bind to AGO1 *in planta*. For this purpose, we first conducted bimolecular fluorescence complementation (BiFC) assays upon *Agrobacterium*-mediated transient transformation of *N. benthamiana* leaves with constructs carrying the N- and C-terminal fragments of the Yellow Fluorescence Protein (YFP) translationally fused to HopT1-1, HopT1-1m3 or Arabidopsis AGO1. In these experiments, we also used split-YFP fusions of HopC1 and of the silencing factor Silencing Defective 3 (SDE3) as negative controls. All these constructs were driven by the moderately active *ubiquitin-10* promoter, which is suitable for transient expression of fluorescently-tagged proteins in *N. benthamiana* (Grefen *et al*., 2010). Confocal imaging revealed a clear fluorescence emission in epidermal cells and guard cells co-expressing either CYFP-HopT1-1/NYFP-AGO1 or NYFP-HopT1-1/CYFP-AGO1 fusions (Figure 2B and 2C), which was significantly different from the baseline fluorescent signal observed in cells co-expressing either CYFP-HopC1/NYFP-AGO1 or NYFP-HopC1/CYFP-AGO1 fusions. Furthermore, the HopT1-1-AGO1 interactions were specific because the fluorescence emission observed upon co-expression of either CYFP-HopT1-1/NYFP-AGO1 or NYFP-HopT1-1/CYFP-AGO1 fusions was significantly different from the weak fluorescent signal detected in cells co-expressing either CYFP-HopT1-1/NYFP-SDE3 or NYFP-HopT1-1/CYFP-SDE3 fusions (Figure 2B and 2C). Collectively, these data indicate that HopT1-1 can specifically interact with AGO1 *in planta*, while the effector HopC1, which cannot suppress miRNA activity nor target AGO1 genetically (Figures 1A and S1A; Navarro *et al*., 2008), is not competent to associate with this silencing factor. It is also noteworthy that our BiFC results never revealed fluorescence signal in the nuclei of *N. benthamiana* epidermal cells co-expressing either CYFP-HopT1-1/NYFP-AGO1 or

NYFP-HopT1-1/CYFP-AGO1 (Figure 2B and 2C), despite the nucleocytoplasmic distribution of GFP-HopT1-1 and of GFP-AGO1 fusions when individually expressed in these cell types (Figure 2D). These observations suggest that HopT1-1 might specifically interact with the cytosolic pool of AGO1, although we cannot exclude that some interaction events additionally occur in the cell nucleus or that the presence of HopT1-1 could interfere with the nuclear localization of AGO1. In addition, we found that the HopT1-1m3 mutant version was not able to interact with AGO1 as revealed by weak fluorescence signal in cells co-expressing either cYFP-HopT1-1m3/nYFP-AGO1 or nYFP-HopT1-1m3/cYFP-AGO1 fusions (Figure 2B and 2C). The latter data indicates that the GW motifs of HopT1-1 are essential to promote the physical association between this bacterial effector and AGO1 *in planta*.

To verify these findings, we next decided to use a non-invasive fluorescence imaging approach by conducting Föster resonance energy transfer-fluorescence lifetime imaging microscopy (FRET-FLIM) analyses after co-expressing a cyan fluorescent protein (CFP)-AGO1 (*35S$_{pro}$:CFP-AGO1*) construct with either *35S$_{pro}$:HopT1-1-YFP* or *35S$_{pro}$:HopT1-1m3-YFP* constructs in *N. benthamiana* leaves. The cytoplasmic HopT1-1-AGO1 interactions that were detected in BiFC (Figure 2B and 2C), prompted us to conduct our FRET-FLIM analyses in this cell compartment. By doing so, we found a significant reduction in the average CFP lifetime in the cytosol of epidermal cells co-expressing CFP-AGO1/HopT1-1-YFP compared with the cytoplasm of epidermal cells co-expressing CFP-AGO1/HopT1-1-HA or expressing CFP-AGO1 alone (Table 1 and Figure S3B), confirming physical interaction between HopT1-1 and AGO1 *in planta*. Furthermore, this protein-protein interaction was fully dependent on the GW motifs of HopT1-1 because we did not detect any FRET in the cytosol of epidermal cells co-expressing CFP-AGO1 and HopT1-1m3-YFP (Table 1

and Figure S3B), which support our BiFC results (Figure 2B and 2C). Altogether, these data provide evidence that HopT1-1 can physically interact with the cytosolic pool of AGO1 and that this process is fully dependent on its AGO-binding platform.

To further confirm the above results *in vitro* and get insights into the contribution of each GW motifs in HopT1-1-AGO1 interaction, we first attempted to produce recombinant GST-HopT1-1 in *Escherichia coli*. However, GST-HopT1-1 was mainly present in the insoluble protein fraction preventing further analysis with the full-length protein (data not shown). To circumvent this problem, we next decided to chemically synthesize biotinylated peptides containing each GW motifs surrounded by native amino acid residues. As a negative control, we synthesized mutated peptides containing tryptophan to phenylalanine substitutions in the tryptophan of each GW motifs (Figure 2E). Equimolar amount of the peptides was bound to streptavidin columns (Figure S5), and then incubated with inflorescence extracts from FLAG-AGO1 transgenic plants. After washing, eluted bound proteins were analyzed by Western blot using anti-FLAG antibody. We observed that HopT1-1 GW2 and GW3 peptides, but not HopT1-1 GW1 peptide, specifically bound to FLAG-AGO1 proteins (Figure 2E). Furthermore, binding to FLAG-AGO1 was partially or completely lost in the presence of the mutated HopT1-1 GF2 and GF3 peptides, respectively (Figure 2E). These additional *in vitro* experiments therefore support our BiFC and FRET-FLIM data and further indicate that HopT1-1 physically interacts with Arabidopsis AGO1, at least in part, through two GW motifs.

HopT1-1 suppresses AGO1-mediated miRNA activity in a GW-dependent manner

To further test the requirement of the GW motifs of HopT1-1 in RNA silencing

suppression, we have analyzed the ability of HopT1-1 and of HopT1-1m3 to suppress AGO1 miRNA activity *in vivo*. For this end, we took advantage of the previously described Arabidopsis *SUC2*$_{pro}$:*amiR-SUL* reporter system in which phloem-specific expression of an artificial miRNA transgene (*amiR-SUL*) triggers silencing of *CHLORINA42* (*CH42*) also known as *SULPHUR* (*SUL*), causing vein-centered chlorosis (Figure 3A and 3B; de Felippes *et al*. 2011). Stable Arabidopsis transgenic *amiR-SUL* lines that overexpress high and comparable levels of HopT1-1 and of HopT1-1m3 transcripts were selected for phenotypical and molecular analyses (Figure S2B). Significantly, transgenic plants overexpressing high levels of HopT1-1 exhibited severe developmental defects (Figures 3A, 5A and S8A) and a compromised vein-centered chlorotic phenotype that was accompanied by an increase in SUL mRNA and protein levels (Figure 3A, 3C and 3E), suggesting that HopT1-1 can suppress *amiR-SUL*-directed silencing of *SUL*. Importantly, these effects were not observed in transgenic plants overexpressing HopT1-1m3 (Figure 3B, 3D and 3E), supporting a role for the HopT1-1 GW motifs in this process. However, additional molecular analyses indicated that the suppression of *amiR-SUL*-mediated silencing of *SUL* triggered by HopT1-1 was not only due to the BSR activity of HopT1-1 but also to the repression of the *SUC2*$_{pro}$:*amiR-SUL* transgene, which was particularly detected in transgenic plants exhibiting dwarf statures (Supplementary text, Figure S6). To further characterize the silencing suppression effects caused by HopT1-1 in a more reliable manner, we next monitored the accumulation of endogenous miRNA targets. We found an enhanced mRNA accumulation of several endogenous miRNA targets in HopT1-1 lines compared with the *SUC2*$_{pro}$:*amiR-SUL* reference line (Figure 3C). Nevertheless, no significant effect was observed on the accumulation of conserved mature miRNAs (Figures S2C;

Navarro *et al*., 2008), nor of the primary miRNA (pri-miRNA) *pri-miR166a* and *pri-miR171c* transcripts, which, as expected, are stabilized in a *dcl1* mutant background (Figure S7). These results indicate that HopT1-1 suppresses AGO1-mediated slicing activity of miRNA targets but does not interfere with miRNA biogenesis nor accumulation. In addition, we noticed that HopT1-1 transgenic lines exhibited a pronounced over-accumulation of the miRNA targets AGO1, AGO2 and DCL1 at the protein level (Figure 3E), despite a lack of effect (for *AGO1* and *DCL1*), or a weak effect (for *AGO2*), on the accumulation of corresponding mRNAs (Figure 3C). By contrast, the level of AGO4 protein, whose cognate mRNAs are not targeted by small RNAs, remained unaltered in HopT1-1 transgenic lines (Figure 3E), which indicates a specific effect of HopT1-1 on miRNA targets. Collectively, these data suggest that HopT1-1 can additionally suppress AGO1-mediated translational inhibition of miRNA targets. Furthermore, in contrast with the above results, we found that stable transgenic plants overexpressing HopT1-1m3 exhibited normal vein-centered chlorosis, with unaltered accumulation of SUL mRNA/protein and of other endogenous miRNA targets (Figures 3B, 3D and 3E), indicating that this mutant version is no longer able to suppress miRNA action. Altogether, these results provide evidence that the GW motifs of HopT1-1 are essential to suppress AGO1-mediated miRNA function *in vivo*.

HopT1-1 suppresses PTI responses in a GW-dependent manner and its presence mimics the impaired PTI responses observed in *ago1* mutants

Given that the majority of *Pto* DC3000 effectors promotes pathogenicity by dampening plant immune responses (Block and Alfano, 2011), we next investigated the ability of HopT1-1 to suppress PTI. Furthermore, the fact that HopT1-1 promotes

pathogenicity through the targeting of AGO1 (Figures 1A, S1A and S1B) prompted us to assess the functional relevance of its AGO-binding platform in this process. Because transgenic plants that constitutively overexpress HopT1-1 exhibit severe developmental defects that preclude the assessment of the possible effects that HopT1-1 could have on PTI responses (Figures 3A and 5A), we decided to generate Arabidopsis stable transgenic plants expressing either Myc-HopT1-1 or Myc-HopT1-1m3 under the dexamethasone (DEX) inducible system (Aoyama and Chua., 1997). Independent transgenic lines expressing comparable protein levels of Myc-HopT1-1 and of Myc-HopT1-1m3 were selected upon DEX application (Figure S4A). It is noteworthy that these reference lines did not exhibit transgene expression in the absence of DEX, indicating that they are not leaky (Figure S4B). We further exploited these genetic resources to test whether HopT1-1 could interfere with PAMP-induced ROS production, which is one of the earliest cellular responses following PAMP perception (Couto and Zipfel., 2016). For this purpose, we challenged these transgenic lines with the flagellin-derived peptide flg22, a well-characterized PAMP surrogate that triggers canonical PTI responses (Felix *et al*., 1999), and further monitored ROS production. In the absence of DEX treatment, we found that both Myc-HopT1-1 and Myc-HopT1-1m3 transgenic lines mount a flg22-induced oxidative burst that was similar to the one observed in WT-elicited plants (Figure S4C). By contrast, when we applied the DEX chemical inducer, we found a strong suppression of flg22-induced ROS production in transgenic lines expressing Myc-HopT1-1 but not in lines expressing Myc-HopT1-1m3 (Figure 4A). These results indicate that HopT1-1 has a potent suppression effect on this early PTI response and that this ability is entirely dependent on functional GW motifs.

To assess whether HopT1-1, and its AGO-binding platform, could interfere with PTI responses in a more physiological context of bacterial infection, we next used the EtHAn system, a recombinant *Pseudomonas fluorescens* strain that can induce classical PTI responses and that expresses a functional type-III secretion system allowing delivery of individual bacterial effectors within host cells (Thomas *et al*. 2009). WT plants were infiltrated with EtHAn alone or with EtHAn strains expressing either HopT1-1 (EtHAn (HopT1-1)) or HopT1-1m3 (EtHAn (HopT1-1m3)) and the production of the reactive oxygen intermediate hydrogen peroxide (H_2O_2) was monitored at 24 hours post-inoculation (Figure 4B). While the EtHAn strain induced strong production of H_2O_2 in WT plants, particularly within and around leaf vasculature, this phenotype was significantly suppressed upon delivery of HopT1-1 (Figure 4B). By contrast, this PTI suppression effect was almost fully abolished upon delivery of the HopT1-1m3 mutant version (Figure 4B), indicating a critical role for the GW motifs of HopT1-1 in this process. In addition, we exploited the EtHAn system to monitor the impact that HopT1-1, and its HopT1-1m3 mutant derivative, could have on bacterial-triggered formation of cell wall deposition of callose, a late PTI response that plays a critical role in the establishment of basal immunity (Hauck *et al*. 2003). Interestingly, we found an ~ 45% decrease in the number of callose deposits in response to EtHAn (HopT1-1) as compared to the EtHAn control, while this PTI suppression effect was not observed upon inoculation of the EtHAn (HopT1-1m3) strain (Figure 4C). Taken together, these data indicate that HopT1-1 can suppress at least two classical PTI responses in a physiological context of bacterial infection. They also provide evidence that the silencing suppression activity of HopT1-1 is coupled with its ability to dampen PTI in Arabidopsis.

Given that AGO1 is a critical target of HopT1-1 (Figures 1 and 2), the above findings suggested a role for AGO1 in orchestrating PAMP-triggered ROS production and callose deposition. To test this possibility, we first monitored flg22-triggered oxidative burst in *ago1-25*, *ago1-26* and *ago1-27* mutant plants. Importantly, all these *ago1* mutants displayed a significantly compromised flg22-induced ROS production as compared to WT-elicited plants (Figure 4D). A significantly impaired flg22-induced ROS production was also detected in the miRNA biogenesis defective mutants *dcl1-11* and *se-1* as compared to WT plants (Figure 4E), indicating that the Arabidopsis miRNA pathway positively regulates this early PTI response. Hydrogen peroxide production and callose deposition were also attenuated in *ago1-27* mutants *versus* WT plants challenged with the EtHAn strain (Figures 4F and 4G), although a milder effect was observed in this mutant background as compared to the effect detected in WT leaves challenged with the EtHAn (HopT1-1) strain (Figure 4B and 4C). These results support a role for AGO1 in PAMP-induced callose deposition, as previously reported during flg22 elicitation (Li *et al*., 2010), but also in ROS production during bacterial elicitation. Altogether, these data suggest that the ability of HopT1-1 to suppress PAMP-triggered ROS production and callose deposition likely involves an inhibitory effect of AGO1 activity.

Expression of *HopT1-1* in Arabidopsis triggers a potent SA-dependent defense response

While generating the HopT1-1 transgenic lines described above (Figure 3), we noticed that transgenic plants expressing high levels of HopT1-1 led to severe plant growth retardation (Figures 3A, 5A and S8A). These phenotypes were reminiscent of the ones observed in autoimmune mutants (Rate *et al*., 1999; Zhang *et al*., 2003), in

which there is constitutive ETI activation. By contrast, transgenic lines expressing the HopT1-1m3 mutant version exhibited normal developmental phenotype (Figures 3B and 5B), indicating that the dwarf phenotype is dependent on the RNA silencing suppression activity of HopT1-1. Based on these observations and on the understanding of the mechanisms required for triggering autoimmune responses (Rate *et al*., 1999; Ji and Ding., 2001; Zhang *et al*., 2003; Zhang *et al*., 2012), we hypothesized that Arabidopsis must have evolved to sense the BSR activity of HopT1-1 and in turn activates a typical SA-dependent defense response similar to ETI. To test this hypothesis, we first monitored the expression of SA-marker genes in plants overexpressing either HopT1-1 or HopT1-1m3. A drastic increased expression of ETI-related markers such as *PATHOGENESIS RELATED 1* (*PR1*), *PR2*, *PR5*, and of the SA-biosynthesis component *ISOCHORISMATE SYNTHASE 1* (*ICS1/SID2*) was detected in HopT1-1- but not in HopT1-1m3-overexpressor plants (Figure 5C). Expression of the cell death and senescence-related marker genes *ALD1* and *WRKY75* (Brosché *et al.,* 2014) was also constitutively high in HopT1-1- but not in HopT1-1m3-overexpressor plants (Figure 5D). Altogether, these results suggested that Arabidopsis has evolved a mechanism to sense the BSR activity of HopT1-1 and in turn activates a SA-dependent defense response.

In Arabidopsis, NLRs are mainly classified into TIR-NB-LRR (TNL) and CC-NB-LRR (CNL) immune-receptors. *PAD4* and *ENHANCED DISEASE SUSCEPTIBLE 1* (*EDS1*) are central components of TNL-immune signaling, while *NDR1* is specifically required for CNL-immune signaling (Cui *et al*., 2015). Furthermore, both TNL- and CNL-immune signaling responses are strongly conditioned by temperature and often abolished at 28°C (Alcazar and Parker, 2011; Chae *et al*., 2014). When HopT1-1-overexpressor plants were grown at 28°C, a significant, albeit not complete,

suppression of the stunted phenotype was observed (Figure 5E), which was associated with a substantial decrease in the basal expression of *PR1* (Figure 5C). This result supports a role for disease resistance proteins in orchestrating HopT1-1-triggered ETI response at 23 °C. To get further genetic evidence for a role of NLR-dependent immune signaling in HopT1-1-induced ETI response, we overexpressed HopT1-1 in a *pad4-1 sid2-2* double mutant (Figure S8B) and further monitored *PR1* expression in this background (Figure S8C). Interestingly, we found a significant decrease in the constitutive expression of *PR1* in this mutant as compared to a reference $35S_{pro}$:*HopT1-1* transgenic plants expressing similar HopT1-1 mRNA level in a $SUC2_{pro}$:*amiR-SUL* (WT) background (Figure 8C). Furthermore, this molecular effect was associated with a partial rescue of plant development (Figures S6A and S8B), further supporting a compromised autoimmune phenotype in the *pad4-1 sid2-2* mutant background. Based on these findings, we conclude that the BSR activity of HopT1-1 induces NLR-dependent signaling, resulting in a strong SA-dependent defense response similar to ETI.

HopT1-1-induced ETI response is correlated with increased accumulation of AGO1, which is sufficient to trigger autoimmunity

Finally, we investigated the possible mechanisms by which the BSR activity of HopT1-1 could trigger ETI. Because overexpression of *NLR* genes is often associated with ETI activation (Oldroyd and Staskawicz, 1998; Tao *et al*., 2000; Zhang *et al*., 2004), we first hypothesized that HopT1-1-induced autoimmunity might be caused by a derepression of Arabidopsis *NLR* gene transcripts that are targeted by small RNAs (Yi and Richards, 2007; Boccara *et al*., 2014; Halter and Navarro, 2015). However, we did not detect a significant stabilization of these transcripts in plants expressing this bacterial effector (Figure S8D), which argues against this

hypothesis. Nevertheless, we cannot exclude that the effect of HopT1-1 on these *NLR* gene products would be only detectable at the protein level as observed for other miRNA targets (Figure 3C and 3E, Navarro *et al*., 2008). Unfortunately, we could not test this hypothesis because of the lack of antibodies raised against these NLR proteins.

Previous molecular analyses showing an over-accumulation of the miRNA targets AGO1, DCL1 and AGO2 in HopT1-1 transgenic plants (Figure 3E), led us to raise another hypothesis, which is not mutually exclusive with the former one. Indeed, we hypothesized that HopT1-1-induced disruption of miRNA-directed control of silencing factor homeostasis, could well be a signal for ETI activation. To test this hypothesis, we decided to alleviate miRNA-directed regulation of one of these RNA silencing factors, namely AGO1, and further determine if such a perturbation could be sufficient to trigger an ETI-like response (Figure 6A). For this purpose, we transformed WT plants with a previously described *AGO1* transgene (*4m*-AGO1), which is refractory to miR168 action due to four silent mutations in miR168 target site (Vaucheret *et al*., 2004), and further analyzed primary transformants exhibiting an enhanced accumulation of AGO1 mRNAs and proteins (Figure 6B). These transgenic lines displayed developmental defects that are associated with a perturbation in miRNA function as previously reported and are referred to as 'mir-AGO1' plants (Vaucheret *et al*., 2004; Figure S9A). We also selected negative controls for these transgenic lines, named 'WT-like' plants, which exhibited a normal developmental phenotype with a mild enhanced accumulation of *AGO1* mRNAs as compared to WT plants (Figure S9A and S9B). Remarkably, the over-accumulation of AGO1 proteins in mir-AGO1 transgenic lines was associated with a constitutive cell death phenotype within and around leaf vasculature that was not observed on leaves of WT-like plants

(Figure 6C). Furthermore, this autoimmune phenotype was accompanied by a drastic enhanced expression of the SA-marker genes *PR1* and to a lesser extent of *PR2*, *PR5*, and *ICS1/SID2* as compared to WT-like plants (Figure 6D) and similar results were obtained when we monitored the expression of the cell death and senescence-related marker genes *ALD1* and *WRKY75* in these plants (Figure 6E). Importantly, this autoimmune phenotype was entirely dependent on the lack of miR168 regulation of the *4m-AGO1* transgene because we found normal developmental phenotype, and WT level of *PR1* and *PR2* transcript accumulation, in Arabidopsis transgenic plants expressing an *AGO1* WT transgene (*WT-AGO1*) that was driven by the same regulatory region than the *4m-AGO1* transgene (Figures S9A, S9B and S9C). Altogether, these results provide compelling evidence that disrupting miR168-directed control of AGO1 homeostasis is sufficient to trigger an ETI-like response in Arabidopsis as observed in HopT1-1 expressing plants.

We further investigated the genetic bases of this autoimmune phenotype. We transformed the miR168-refractory *AGO1* transgene in the *ndr1-1*, *sid2-2* and *pad4-1 sid2-2* mutant backgrounds and selected transgenic lines exhibiting strong and comparable *AGO1* mRNA levels (Figures 6B and S9D). The constitutive expression of defense-, cell death- and senescence-associated- marker genes observed in mir-AGO1 WT plants was partially suppressed in *ndr1-1* and *sid2-2* mutant backgrounds (Figures S9D and S9E), supporting a role for CNLs and SA-biosynthesis in the autoimmune phenotype. Messenger RNA accumulation of these marker genes was even further compromised in the *pad4 sid2* mutant background (Figures 6D, 6E, S5D and S9E), indicating an additional –and likely predominant– role for TNL-immune signaling in the ETI phenotype triggered in mir-AGO1 plants. Consistently, we observed that the constitutive *PR1* expression detected in mir-AGO1 WT plants was

impaired at 28°C as compared to 23°C conditions (Figure S9F). Altogether, these results indicate that perturbing miR168-directed control of AGO1 homeostasis is sufficient to trigger CNL/TNL-immune signaling, which in turn results in a potent SA-dependent defense response. These results also suggest that HopT1-1-induced suppression of miR168-directed control of AGO1 homeostasis might contribute to the ETI response triggered by this BSR.

DISCUSSION

In the present study, we have demonstrated a key role for the Arabidopsis miRNA pathway in PAMP-induced ROS production, a well-characterized PTI response that occurs within minutes of PAMP detection and that plays a crucial role in antibacterial defense (Couto and Zipfel., 2016; Torres *et al*., 2006). We have shown that the Arabidopsis miRNA factors DCL1, SE and AGO1 are all required for flg22-induced oxidative burst (Figure 4E). Furthermore, we found that the EtHAn strain triggers an intense accumulation of H_2O_2 within and around Arabidopsis leaf vasculature, a phenotype that was partially impaired in an *ago1* mutant background (Figure 4F). Such AGO1-dependent regulatory process might ensure the formation of an immune cell layer adjacent to the vasculature to limit bacterial spreading from xylem vessels to mesophyll cells and *vice versa*. In addition, this phenomenon might result in an enhanced accumulation of H_2O_2 in xylem vessels, thereby potentially reducing bacterial survival through the well-characterized bactericidal function of this reactive oxygen intermediate (Hong *et al*., 2013). Such an antibacterial activity would notably be relevant to control *Pto* DC3000 pathogenesis because this bacterium was previously shown to propagate through xylem vessels in both Arabidopsis and *N. benthamiana* (Yu *et al*., 2013; Misas-Villamil *et al*., 2011). Although the detailed

mechanisms by which the Arabidopsis miRNA pathway orchestrates ROS production remains to be established, we propose that miRNA-dependent control of PTI repressors such as Auxin Response Factors 16 and 17 could contribute to this process (Li *et al*., 2010; Figure 7). Furthermore, because PAMP-induced oxidative burst is a very rapid response, we suggest that miRNA-directed control of ROS production might additionally be caused by the action of a pre-loaded AGO1-miRISC that would operate at the level of early PTI signaling events, an intriguing possibility that will deserve attention in the future.

Given that the Arabidopsis miRNA pathway is a major component of PTI (Navarro *et al*., 2008; Li *et al*., 2010; this study), it is likely that many pathogen effectors will be found to target this small RNA pathway to enable disease. Consistent with this idea, we have previously identified type-III secreted proteins from *Pto* DC3000 that suppress all the steps of the Arabidopsis miRNA pathway (Navarro *et al*., 2008; unpublished data). However, until now, it was unknown if some of these BSRs could directly interfere with component of the RNA silencing machinery to suppress miRNA activity and cause disease. In the present work, we showed that the bacterial effector HopT1-1 is a critical virulence determinant that promotes growth of *Pto* DC3000 in a physiological context of infection (Figure 1). Importantly, the reduced growth of the *hopT1-1*-deleted strain was entirely rescued in miRNA-defective mutants including *ago1* (Figures 1 and S1), providing evidence that the Arabidopsis AGO1-dependent miRNA pathway is a major genetic target of HopT1-1. In agreement with these functional analyses, we showed that HopT1-1 can physically interact with Arabidopsis AGO1, at least in part, through two conserved GW motifs (Figure 2). Furthermore, GW motifs of HopT1-1 were found to be not only essential for the

suppression of miRNA activity but also for the dampening of PAMP-triggered ROS production and callose deposition in Arabidopsis (Figures 3 and 4). This implies that the BSR activity of HopT1-1 is directly coupled with its ability to suppress PTI. This phenomenon might be due to HopT1-1-induced derepression of negative regulators of PTI that are controlled by miRNAs as previously mentioned (Figure 7). Future investigations will be required to determine the detailed mode of action of HopT1-1 once recruited onto AGO1-RISC. For instance, it will be essential to determine if HopT1-1 could possess an enzymatic activity outside of its AGO-binding platform to impede AGO1 activity and whether this bacterial effector could prevent and/or displace the interaction between AGO1 and yet-unknown endogenous Arabidopsis GW/WG miRNA factors during bacterial infection.

In addition, we have shown that the constitutive expression of HopT1-1 in plants triggers an over-accumulation of AGO1, AGO2 and DCL1, which is normally negatively regulated by miR168, miR403 and miR162/838, respectively (Rajagopalan *et al*., 2006; Xie *et al*., 2003; Vaucheret *et al*., 2004). Interestingly, this molecular effect was accompanied by a strong autoimmune phenotype that was dependent on CNL- and TNL-immune signaling factors (Figures 5 and S8). Importantly, both the HopT1-1-induced over-accumulation of the above silencing factors and the HopT1-1-triggered autoimmune phenotype were dependent on the BSR activity of this effector (Figures 3, 5 and S8). These observations suggest that HopT1-1-induced suppression of miRNA activity might be causal for silencing factor over-accumulation and ETI activation. Consistent with this hypothesis, we found that transgenic plants expressing an *AGO1* transgene that is refractory to miR168 action trigger a strong over-accumulation of AGO1 that was associated with a potent CNL/TNL-dependent autoimmune phenotype (Figure 6 and S9). These results provide evidence that

HopT1-1-induced disruption of miR168-directed control of AGO1 homeostasis is a trigger of ETI activation. Furthermore, given that AGO1 is (1) indispensable for the virulence function of HopT1-1 (Figure 1), (2) a critical PTI factor (Figure 4, Li *et al*., 2010), (3) directly targeted by HopT1-1 as well as several other VSRs (Figure 2, Pumplin and Voinnet, 2013), and (4) misregulated by HopT1-1 through a disruption of miR168 activity, we propose that AGO1 likely represents a guarded HopT1-1 target. In this scenario, some NLR proteins would have evolved to monitor the integrity of AGO1 homeostasis, and trigger a SA-dependent ETI response upon HopT1-1-induced disruption of miR168 activity (Figure 7). Future studies should identify and characterize the CNLs and TNLs that are associated with AGO1 and that can monitor the integrity of AGO1 homeostasis. In addition, even though we could not detect significant changes of a subset of *NLR* gene transcripts that are controlled by small RNAs in HopT1-1 transgenic lines (Figure S8C), we do not rule out the possibility that HopT1-1 could enhance the protein level of some of these immune receptors, or of other NLRs/positive regulators of ETI controlled by small RNAs, which would contribute to ETI activation.

Although we have shown that HopT1-1 can induce ETI when overexpressed *in planta* (Figures 5 and S8), we found that deletion of this effector in *Pto* DC3000 leads to a significant decrease in bacterial titer in the susceptible Arabidopsis Col-0 accession (Figures 1 and S1). This counter-intuitive result suggests that the level and/or secretion of HopT1-1 are likely under tight regulatory control so that a restricted amount of this effector is delivered in host cells during bacterial infection. Such an amount, if properly distributed within host cells, could be sufficient to trigger PTI suppression while limiting HopT1-1-induced ETI response. Future experiments will

be necessary to test this hypothesis. It will also be interesting to determine if some other natural accessions of *Arabidopsis thaliana* could have evolved *NLR* gene alleles that are more prone to detect the silencing suppression activity of HopT1-1 in a physiological context of bacterial infection.

Our study suggests that the homeostasis of AGO1 is likely under tight regulatory control in normal growth conditions so that plants can mount a robust host counter-counter defense specifically upon pathogen-induced suppression of miR168 activity. Such pathogen detection mechanism might not only operate in response to the BSR HopT1-1 but also potentially in the presence of some VSRs. Intriguingly, the helper component-protease (Hc-Pro), which was found to trigger enhanced AGO1 protein accumulation *in planta* (Chiu *et al*., 2010; Ivanov *et al*., 2016), can promote disease resistance towards unrelated pathogens in tobacco through SA-dependent and SA-independent responses (Pruss *et al*., 2004). Although the initial trigger of such Hc-Pro-triggered disease resistance mechanism remains elusive and might rely on the derepression of *R* gene transcripts that are controlled by small RNAs (Yi and Richards, 2007), our work suggests that the known stabilization of AGO1 triggered by this VSR might contribute this process. On the other hand, the pathogen-detection mechanism described in the present study implies that some successful pathogens must have evolved ways to buffer the perturbation of AGO1 homeostasis caused by pathogen-triggered suppression of miR168 activity, thereby dampening such host-counter-counter defense. Consistent with this idea, several plant RNA viruses, but also the well-characterized Tombusvirus VSR p19, were shown to trigger enhanced miR168 accumulation leading to a reduction in AGO1 protein levels (Várallyay *et al*., 2010), a regulatory process which was not observed in response to HopT1-1 (Figure

S2C). Based on these findings and on the present work, we propose that viral-induced accumulation of miR168 is likely an important strategy employed by viruses not only to counteract the anti-viral function of AGO1, as previously suggested, but also potentially to prevent ETI activation triggered by a misregulation of AGO1 homeostasis.

The present study reveals that the use of GW/WG-dependent AGO-binding platforms is not restricted to VSRs, as previously described (Azevedo *et al*., 2010; Karran and Sansfaçon, 2014; Aqil *et al*., 2013; Giner *et al*., 2010), but can also be exploited by a functionally relevant bacterial effector. Intriguingly, we have also retrieved GW/WG motifs in an appropriate sequence context in secreted effectors from various phytopathogenic bacteria, fungi and oomycetes (Figure S10). For instance, we could identify the presence of canonical GW/WG motifs in effectors from the devastating plant bacterial vascular pathogens *Xylella* and *Xanthomonas* or from the oomycetes *Phytophthora sojae* and the Irish potato famine pathogen *Phytophthora infestans* (Figure S10). Canonical GW/WG motifs were also retrieved in fungal effectors produced by the wheat stem rust pathogen *Puccinia graminis* f. sp. *tritici*, which represents one of the most destructive pathogen of wheat worldwide, but also by *Fusarium graminearum*, which is the causal agent of Fusarium head blight that causes serious yield losses in wheat and barley worldwide (Figure S10). Collectively, these observations suggest that a wide range of non-viral phytopathogens might have evolved an analogous mode of action to promote pathogenicity in agriculturally relevant crops. It will thus be interesting to establish if the discoveries made on HopT1-1 hold for other silencing suppressors derived from non-viral phytopathogens.

MATERIALS AND METHODS

DNA Contructs

The pK7WG2D destination vector carrying the *HopT1-1* gene was previously described (Navarro *et al.*, 2008). To generate the mutated versions of HopT1-1, GW>GF substitutions in the *HopT1-1* ORF were carried out by PCR-based site-directed mutagenesis using mismatched primers. The resulting PCR product was introduced in the pENTR/D-TOPO entry vector, sequenced and then recombined into the GATEWAY Binary destination vector pK7WG2D to overexpress untagged protein. To overexpress tagged protein of WT and mutant versions of HopT1-1, the above pENTR vectors were recombined into the GATEWAY Binary destination vector pEarleyGate203 (N-terminal Myc tag). To generate DEX_{pro}:*Myc-HopT1-1* (WT) and DEX_{pro}:*Myc-HopT1-1m3* (GW>GF) constructs, the pEarleyGate203 plasmids containing HopT1-1 or HopT1-1m3 versions were used to amplify Myc-HopT1-1 and Myc-HopT1-1m3 sequences that were digested with SpeI and ligated into the corresponding site of the binary vector pTA7002 carrying the DEX-inducible promoter (Aoyama and Chua, 1997). To overexpress HopT1-1 and HopT1-1m3 in the EtHAn system (Thomas *et al*, 2009), versions of HopT1-1 and HopT1-1m3 without a stop codon were cloned in the pENTR/D-TOPO entry vector that was further recombined into the destination vector pBS0046 containing the NPTII promoter. For the BiFC assays, the coding regions of *AGO1*, *SDE3*, *HopT1-1*, *HopT1-1m3* and *HopC1* were first cloned into the pDON207 plasmid and further recombined into the GATEWAY BiFC binary destination vectors pUBN-YFP containing the N-ter or the C-ter part of YFP protein that were previously described in Grefen *et al.* (2010). For the subcellular localization of GFP, HopT1-1 and HopT1-1m3, the pDON-GFP, pDON-

HopT1-1 and pDON-HopT1-1m3 were recombined into the GATEWAY pB7WGF2 plasmid. For the FRET/FLIM experiment, the no stop versions of pDON-HopT1-1 and pDON-HopT1-1m3 were recombined into the destination vector pBin-35S-GWY-YFP. All the constructs inserted in GATEWAY binary destination vectors were transformed into the *Agrobacterium tumefaciens* strains GV3101 or C58C1.

Transgenic plants and mutants

Arabidopsis thaliana silencing defective mutants *ago1-25, ago1-26, ago1-27*, *ago2-1*, *ago4-2*, *ago4-3*, *dcl2-1 dcl4-2*, *se-1*, *dcl1-11*, *sgs3-1*, *rdr1-1 rdr2-1 rdr6-15* and the *SUC2*$_{pro}$:*amiR-SUL* silencing reporter line were previously described (Morel *et al.*, 2002; Agorio and Vera, 2007; Havecker *et al.*, 2010; Henderson *et al.*, 2006; Zhang *et al.*, 2008; Mourrain *et al.*, 2000; Garcia-Ruiz, 2010; de Felippes *et al.*, 2011). The *SUC2*$_{pro}$:*amiR-SUL* line was transformed with pK7WG2D carrying HopT1-1 or HopT1-1m3 constructs. Independent T2 transgenic lines expressing HopT1-1 or HopT1-1m3 at the same levels were selected. To generate DEX-inducible transgenic plants, pTA7002 vectors carrying Myc-HopT1-1 or Myc-HopT1-1m3 were transformed in the Arabidopsis Col-0 accession. Two independent T2 transgenic lines expressing Myc-HopT1 or Myc-HopT1-1m3 proteins at the same level were selected and used in this study. To generate plants expressing constitutively Myc-HopT1-1 and Myc-HopT1-1m3, pEarleyGate203 vectors carrying Myc-HopT1-1 or Myc-HopT1-1m3 were transformed in Col-0 and multiple T1 primary transformants were analyzed. These constructs were also transformed in *pad4 sid2* mutant background. The construct containing an *AGO1* gene refractory to miR168 cleavage (*4m-AGO1*) was described in Vaucheret *et al.* (2004) and transformed in Col-0, *ndr1-*

1, *sid2-2* or *pad4 sid2* mutants. Analysis was done in multiple T1 primary transformants grown at different growth temperatures (23°C or 28°C).

Bacterial strains

The bacterial strains used in this study include *Pseudomonas syringae* pv. *tomato* DC3000 (*Pto* DC3000), *hopT1-1*-deleted strain (*Pto* Δ*hopT1-1*) and *hopC1*-deleted strain (*Pto ΔhopC1*). These bacterial strains were grown at 28°C in NYGB medium (5 g L^{-1} bactopeptone, 3 g L^{-1} yeast extract, 20 ml L^{-1} glycerol) containing rifampicin (25 µg/mL) for selection. The *Pto ΔhopT1-1* was generated by an unmarked mutagenesis strategy described by House *et al.* (2004) with some modifications. Briefly, DNA regions upstream and downstream of *hopT1-1* were amplified with primer pairs P4835/P4836 and P4837/P4838 (Table S1), respectively. The resulting PCR fragments were cloned into pENTR/D-TOPO (Invitrogen, Carlsbad, CA) and then recombined into suicide destination vector pMK2016 for the upstream construct or pMK2017 for the downstream construct, using LR Clonase (Invitrogen, Carlsbad, CA) according to the manufacturer's instructions resulting in constructs pLN5426 and pLN5472, respectively. Constructs pLN5426 and pLN5472 were integrated into the *Pto* DC3000 chromosome by biparental or triparental mating. Plasmid pBH474, which contains a gene encoding the yeast FLP recombinase, was introduced into the resulting strains to excise the integrated plasmid at FLP recombinase target (FRT) sequences. To cure pBH474, isolated colonies were spread on King's B medium (King *et al.,* 1954) agar plates containing rifampicin (100 µg/mL) with 5% sucrose. PCR primer pair P4839/P4840 (Table S1) was used to identify mutants that carried the *hopT1-1* deletion.

The *Pto ΔhopC1* was generated by an insertional mutagenesis strategy described by Windgassen *et al.* (2000) with some modifications. Briefly, an internal fragment within the *hopC1* coding region was amplified with primer pair P164/P165 (Table S1). The resulting PCR fragment was cloned into a suicide vector pKnockout-Ω that had been digested with XcmI, resulting in construct pLN6. Construct pLN6 was integrated into the *Pto* DC3000 chromosome by triparental mating using spectinomycin (50 µg/mL) to select for the plasmid marker. PCR primer pair P181/P165 was used to identify mutants that contained an integrated pKnockout-Ω in *hopC1*.

Plant Growth Conditions and Treatments

Plants used in this study were grown in incubation chambers at 19–23 °C (dark/light) with an 8-h photoperiod for most assays except for the two-week-old seedlings of $SUC2_{pro}$*:amiR-SUL* and transgenic lines expressing HopT1-1 or HopT1-1m3 in $SUC2_{pro}$*:amiR-SUL* background, which were transferred from 23°C to 28°C. Transgenic plants expressing HopT1-1, under the control of the DEX inducible promoter (DEX_{pro}) or the constitutive CAMV 35S ($35S_{pro}$), were selected on plates containing Murashige and Skoog medium (Duchefa) [composition for a 1-L medium (pH = 5.7): 2.3 g MS, 0.5% sucrose, 0.8% agar, 0.5 g MES, vitamins (Sigma)] in presence of Hygromycin B (10 µg/mL) or Kanamycin (50 µg/mL), respectively and then transferred to soil 15 day-post-germination (dpg). Experiments conducted in DEX_{pro}*:Myc-HopT1-1* and DEX_{pro}*:Myc-HopT1-1m3* transgenic plants were performed on five-week-old plants sprayed every 24 hours, with 30 µM of dexamethasone (DEX; Sigma) in the presence of 0.01% Tween 20 and/or subsequently challenged 48 hours after with either water or 100 nM of flg22 peptide (QRLSTGSRINSAKDDAAGLQIA, GenScript®). *Nicotiana benthamiana* plants for

transient expression assays were grown in growth chamber at 19-23°C (dark/light) with a 16 hours photoperiod.

Bacterial growth assays

Five-week-old Col-0 Arabidopsis (WT) or the mutant plants were covered with a lid 24 hours under high humidity before to be dip-inoculated with *Pto* DC3000 WT, *Pto ΔhopT1-1* or *Pto ΔhopC1* at 10^8 cfu/mL with 0,02% of Silwet L-77 (Lehle Seeds). Dip-inoculated plants were allowed to stay under high humidity condition for 3 days before the bacterial counting was performed. For each condition, around 15 leaves from three plants were collected and the following steps were performed as described in Navarro *et al.* (2008).

***Agrobacterium*-mediated transient expression**

Agrobacterium tumefaciens strains carrying the indicated plasmids were inoculated in 10 ml of LB medium supplied with rifampicin and the other selective antibiotic and placed in an incubator shaker (200 rpm) at 28°C overnight. Cells were harvested by centrifugation at 4500 rpm and resuspended to a final optical density at 600 nm (OD_{600}) of 0.2 in a solution containing 10 mM MES, pH 5.6, 10 mM $MgCl_2$ and 200 μM acetosyringone. Cultures were incubated in the dark at room temperature for 5 hours before agro-infiltration. For the co-infiltration of two different *A. tumefaciens* strains, equal concentrations (OD_{600}: 0.25) of both the cultures were mixed before agro-infiltration of leaves of four-week-old *Nicotiana benthamiana* plants. Infiltrated plants were covered with a lid and the leaves were collected and flash frozen 48-72 hours post infiltration. Confocal image analyses for the subcellular localization and for the BiFC experiments were performed 2-3 days post infiltration. YFP fluorescence for

each sample was visualized and acquired by using Leica SP5 and SP8 confocal microscopes and quantification of the fluorescence signal for each picture taken (n=10) was performed using ImageJ software.

Semi-quantitative PCR analysis

Total RNA was extracted using RNeasy Plant Mini kit (Macherey-Nagel) followed by DNAse (Promega) digestion at 37°C to remove the genomic DNA. 0.5 µg of DNA-digested RNA was used to reverse-transcribe into cDNA using qScript cDNA Supermix (Quanta Biosciences). The *pri-miR166a* and *pri-miR171c* transcripts were amplified using 28 cycles and 35 cycles, respectively, to perform semi-quantitative PCR analysis according to Navarro *et al.* (2008). Quantification was done by amplifying *ubiquitin10* transcripts with 28 cycles. Specific primers (Barciszewska-Pacak *et al.* (2015) were used and are listed in Table S1.

Quantitative Real Time PCR analysis

Total RNA was extracted using RNeasy Plant Mini kit (Macherey-Nagel) followed by DNAse (Promega) digestion at 37°C to remove the genomic DNA. 0.5 µg of DNA-digested RNA was used to reverse-transcribe into cDNA using qScript cDNA Supermix (Quanta Biosciences). The cDNA was quantified using a SYBR Green qPCR mix (Takyon; Eurogentec) and gene-specific primers. PCR was performed in 384-well plates heated at 95 °C for 10 min, followed by 45 cycles of denaturation at 95 °C for 10 s and annealing at 60 °C for 40 s. A melting curve was performed at the end of the amplification. Transcript levels were normalized to that of *Actin2* and/or *Ubiquitin*. Primers used to monitor *Actin2*, *SPL10*, *ARF17, ALD1, PLP2, RPS5, RSG1, RSG2, SNC1* and *RPP4* were previously described (Navarro *et al.*, 2008;

Zhang *et al.*, 2008; La Camera *et al.*, 2009; Acharya *et al.*, 2007; Brosche *et al.*, 2014; Boccara *et al.*, 2014; Yi *et al.*, 2007). Primer pairs used for the remaining genes are listed in Table S1.

RT-qPCR analysis on mature miRNAs

Briefly, RNA was extracted using TRizol reagent (Invitrogen), and then 0.5 µg of DNA-digested RNA was used to perform reverse transcription (qSCRIPT, Quanta Biosciences) using a stem-loop-adapter primer specific to the miRNA, as described in Varkonyi-Gasic *et al.* (2007) (see Table S1). 200 pg of cDNA was used to do a 2-step qPCR analysis with the universal reverse primer coupled with the forward primer specific to the miRNA (see Table S1).

Proteins extraction and analyses

Total protein extracts were resolved on SDS-PAGE after quantification with Bradford Assay. After electroblotting proteins on Nitrocellulose membrane (Millipore), protein blot analysis was performed using antiserum to specific antibodies.

Pull-down experiments

Biotinylated peptides (synthetized by Eurogentec, sequences shown in Figure 3) were quite insoluble in water and were resuspended in 6M urea, and sonicated four times (Bioruptor^{TM}, Diagenode, 30s on/1min off on High). They were quantified at 205 nm using the Nanodrop 2000 according to manufacturer's instruction (Thermoscientific) and checked by dot blot analysis. The solubilized peptides were spotted on to the nitrocellulose membrane at three different amounts (1 µg, 0.1 µg and 0.01 µg) and were detected by using the streptavidin protein conjugated to HRP

(ref 21126, Thermoscientific), and then was developed using the ECL substrate. For binding assays, 10 µg of peptides were diluted into 450 µL of PBS containing 0.1% NP-40 and were incubated 30 min at room temperature in the presence of 0.9 mg of Dynabeads® MyOne™ Streptavidin T1. The beads were then washed once in 0.1% NP-40 PBS and twice in IP buffer (10% glycerol, 50mM Tris-HCl pH 7.4, 150mM NaCl, 5mM $MgCl_2$, 0.1% NP-40, 2 mM DTT, EDTA-free complete Protease Inhibitor Cocktail (Roche). They were incubated in the presence of inflorescence extracts from Flag-AGO1 Arabidopsis plants in IP buffer for 2 hours at 4°C. After 3 washes of the beads in IP buffer, the proteins were eluted in Laemmli buffer and resolved in a 6% SDS-PAGE gel. The AGO1 protein was detected by Western blot using a Flag-HRP antibody (A8592, Sigma).

FRET-FLIM Measurement

Fluorescence lifetime measurements were performed in time domain using a streak camera (Camborde *et al.,* 2017). The light source is a 440 nm pulsed laser diode (PLP-10, Hamamatsu, Japan) delivering ultrafast picosecond pulses of light at a fundamental frequency of 2 MHz. All images were acquired with a 60x oil immersion lens (plan APO 1.4 N.A., IR) mounted on an inverted microscope (Eclipse TE2000E, Nikon, Japan). The fluorescence emission is directed back into the detection unit through a short pass filter and a band pass filter (490/30 nm). The detector is a streak camera (Streakscope C4334, Hamamatsu Photonics, Japan) coupled to a fast and high-sensitivity CCD camera (model C8800-53C, Hamamatsu). For each acquisition, average fluorescence decay profiles were plotted and lifetimes were estimated by fitting data with exponential function using a non-linear least-squares estimation procedure (Camborde *et al.*, 2017). Fluorescence lifetime of the donor

was experimentally measured in the presence and absence of the acceptor. FRET efficiency (E) was calculated by comparing the lifetime of the donor in the presence (τ_{DA}) or absence (τ_D) of the acceptor: $E=1-(\tau_{DA})/(\tau_D)$. Statistical comparisons between control (donor) and assay (donor + acceptor) lifetime values were performed by Student *t* test.

Quantification of flg22-induced ROS production

For each condition, discs (0.4 cm in diameter) of leaf tissue were harvested from three individual five-week-old plants and incubated in water in 96-well plates overnight in a growth chamber at 23°C. After 24 hours, 100 µL H_2O containing 20 µM luminol and 1 µg horseradish peroxidase (Sigma) with 100 nM flg22 was added to replace the water used for overnight incubation. Luminescence (relative light units) was immediately measured for a time-course of 45 min using a Tristar LB 941 plate reader (Berthold technologies).

Callose deposition

Five-week-old Arabidopsis Col-0 (WT) plants or *ago1-27* mutant plants were infiltrated with 10 mM of $MgCl_2$ or 10^8 cfu/mL of EtHAn strains. Seven hours after infiltration, around 12 leaves were collected from three independent plants and incubated overnight in lactophenol (1 volume of glycerol:lactic acid:phenol:water, ratio 1:1:1:1, and 2 volumes of EtOH). After washing steps in EtOH 50% followed by in water, leaves were incubated for 30 min in aniline blue staining solution (K_2HPO_4 150 mM pH 9.5 with 0.01% aniline blue). Leaves were mounted with 50% glycerol and visualized with Olympus Macro Zoom System Microscope MVX10 fluorescent microscope (excitation filter 365 nm and barrier filter 420 nm). The number of callose

deposits was quantified using ImageJ software (National Institutes of Health, Bethesda). Forty fields of view (each 0.56 mm^2) were analyzed and averaged.

DAB staining

Five-week-old Arabidopsis Col-0 (WT) plants or *ago1-27* mutant plants were infiltrated with 10 mM of $MgCl_2$ or 10^8 cfu/mL (OD_{600}: 0.2) of EtHAn strains. After 48 hours, the infiltrated leaves were collected and vacuum-infiltrated with DAB staining buffer (1 mg/mL, pH 3.5) and then incubated for 5 hours in the same buffer. Leaves were boiled for 15 min in EtOH:glycerol:acid lactic (ratio 4:1:1), washed overnight in EtOH and then mounted with 50% glycerol and further visualized using Olympus Macro Zoom System Microscope MVX10. The intensity of DAB staining was quantified with ImageJ software (National Institutes of Health). Forty fields of view (each 0.56 mm^2) were analyzed and averaged.

Trypan blue staining

Leaves from five eight-week-old Arabidopsis Col-0 (WT) plants or mir-AGO1 plants were placed in a 15 ml tube and immersed in lactophenol trypan blue solution (acid lactic/ glycerol/phenol/water/trypan blue: ratio 1:1:1:1; diluted before use at a ratio 1:1 with EtOH). The tube was placed into a boiling water bath for 2 min followed by destaining in 5 ml chloral hydrate solution (2.5 g/mL water) for 2 hours and a second time overnight on an orbital shaker. Note that the staining step should not exceed the time indicated to avoid a strong background signal. After extensive washes in water, the leaves were mounted onto glass microscope slides in presence of 50% glycerol and examined using Olympus Macro Zoom System Microscope MVX10.

REFERENCES

Agorio, A., and Vera, P. (2007). ARGONAUTE4 is required for resistance to *Pseudomonas syringae* in Arabidopsis. The Plant Cell *19*, 3778-3790.

Alcazar, R., and Parker, J.E. (2011). The impact of temperature on balancing immune responsiveness and growth in Arabidopsis. Trends in plant science *16*, 666-675.

Aoyama, T. and Chua, N.H. (1997). A glucocorticoid-mediated transcriptional induction system in transgenic plants. Plant Journal 11, 605-612.

Aqil, M., Naqvi, A.R., Bano, A.S., and Jameel, S. (2013). The HIV-1 Nef protein binds argonaute-2 and functions as a viral suppressor of RNA interference. PLoS one *8*, e74472.

Acharya, B. R., S. Raina, S. B. Maqbool, G. Jagadeeswaran, S. L. Mosher, H. M. Appel, J. C. Schultz, D. F. Klessig, and R. Raina. 2007. "Overexpression of CRK13, an Arabidopsis cysteine-rich receptor-like kinase, results in enhanced resistance to Pseudomonas syringae." *Plant J* 50 (3):488-99.

Azevedo, J., Garcia, D., Pontier, D., Ohnesorge, S., Yu, A., Garcia, S., Braun, L., Bergdoll, M., Hakimi, M.A., Lagrange, T., et al. (2010). Argonaute quenching and global changes in Dicer homeostasis caused by a pathogen-encoded GW repeat protein. Genes & Dev. 24, 904-915.

Azevedo, J., Cooke, R., and Lagrange, T. (2011). Taking RISCs with Ago hookers. Curr Opin Plant Biol. *14*, 594-600.

Barciszewska-Pacak M., Milanowska K., Knop K., Bielewicz D., Nuc P., Plewka P., Pacak A.M., Vazquez F., Karlowski W., Jarmolowski A., and Szweykowska-Kulinska Z. (2015). Arabidopsis microRNA expression regulation in a wide range of abiotic stress responses. Front Plant Sci. *4,* 6:410.

Baulcombe, D.C. (2015). VIGS, HIGS and FIGS: small RNA silencing in the interactions of viruses or filamentous organisms with their plant hosts. Current opinion in plant biology *26*, 141-146.

Baumberger, N., and D. C. Baulcombe. 2005. "Arabidopsis ARGONAUTE1 is an RNA Slicer that selectively recruits microRNAs and short interfering RNAs." *Proc Natl Acad Sci U S A* 102 (33):11928-33.

Block, A. and Alfano, JR. (2011). Plant targets for *Pseudomonas syringae* type III effectors: virulence targets or guarded decoys? Cell Opin Microbiol *14*, 39-46.

Boccara, M., Sarazin, A., Thiébeauld, O., Jay, F., Voinnet, O., Navarro, L., Colot, V. (2014). The Arabidopsis miR472-RDR6 silencing pathway modulates PAMP- and effector-triggered immunity through the post-transcriptional control of disease resistance genes. PLoS Pathog. *10*, e1003883.

Bologna, N.G., and Voinnet, O. (2014). The diversity, biogenesis, and activities of endogenous silencing small RNAs in Arabidopsis. Annual review of plant biology *65*, 473-503.

Brodersen, P., Sakvarelidze-Achard, L., Bruun-Rasmussen, M., Dunoyer, P., Yamamoto, Y.Y., Sieburth, L., and Voinnet, O. (2008). Widespread translational inhibition by plant miRNAs and siRNAs. Science *320*, 1185-1190.

Brosché, M., Blomster, T., Salojarvi, J., Cui, F., Sipari, N., Leppala, J., Lamminmaki, A., Tomai, G., Narayanasamy, S., Reddy, R.A., et al. (2014). Transcriptomics and functional genomics of ROS-induced cell death regulation by RADICAL-INDUCED CELL DEATH1. PLoS genetics *10*, e1004112.

Brosseau, C., El Oirdi, M., Adurogbangba, A., Ma, X., and Moffett, P. (2016). Antiviral Defense Involves AGO4 in an Arabidopsis-Potexvirus Interaction. Molecular plant-microbe interactions : MPMI *29*, 878-888.

Camborde L., Jauneau A., Brière C., Deslandes L., Dumas B., Gaulin E. (2017). Detection of nucleic acid-protein interactions in plant leaves using fluorescence lifetime imaging microscopy. Nat Protoc. 12(9):1933-1950.

Carbonell, A., Fahlgren, N., Garcia-Ruiz, H., Gilbert, K.B., Montgomery, T.A., Nguyen, T., Cuperus, J.T., and Carrington, J.C. (2012). Functional analysis of three Arabidopsis ARGONAUTES using slicer-defective mutants. The Plant cell *24*, 3613-3629.

Chae, E., Bomblies K., Kim, S-T., Karelina, D., Zaidem, M., Ossowski, S., Martin-Pizarro, C., Laitinen, R.A.E., Rowan, B.A., Tenenboim, H., Lechner, S., Demar, M., Habring-Müller, A., Lanz, C., Rätsch, G., and Weigel, D. (2014). Species-wide genetic incompatibility analysis identified immune genes as hot spots of deleterious epistasis. Cell 159, 1341-1351.

Chiu, D-H., Chen I-H., Baulcombe, D., Tsai, C-H. (2010). The silencing suppressor P25 of potato virus X interacts with Argonaute 1 and mediates its degradation through the proteasome pathway. Molecular Plant Pathology. *11*, 641-659.

Chen, X. (2004). A microRNA as a translational repressor of APETALA2 in Arabidopsis flower development. Science *303*, 2022-2025.

Couto, D., Zipfel, C. (2016). Regulation of pattern recognition receptor signaling in plants. Nat Rev Immunol. 16, 537-552.

Cui, H., Tsuda, K., and Parker, J.E. (2015). Effector-triggered immunity: from pathogen perception to robust defense. Annual review of plant biology *66*, 487-511.

Dalmay, T., Hamilton, A., Rudd, S., Angell, S., and Baulcombe, D.C. (2000). An RNA-dependent RNA polymerase gene in Arabidopsis is required for posttranscriptional gene silencing mediated by a transgene but not by a virus. Cell *101*, 543-553.

Dangl, J.L., and Jones, J.D. (2001). Plant pathogens and integrated defence responses to infection. Nature *411*, 826-833.

de Felippes, F.F., Ott, F., and Weigel, D. (2011). Comparative analysis of non-autonomous effects of tasiRNAs and miRNAs in Arabidopsis thaliana. Nucleic acids research *39*, 2880-2889.

Deleris, A., Gallego-Bartolome, J., Bao, J., Kasschau, K.D., Carrington, J.C., and Voinnet, O. (2006). Hierarchical action and inhibition of plant Dicer-like proteins in antiviral defense. Science *313*, 68-71.

Derrien, B., Baumberger, N., Schepetilnikov, M., Viotti, C., De Cillia, J., Ziegler-Graff, V., Isono, E., Schumacher, K., and Genschik, P. (2012). Degradation of the antiviral component ARGONAUTE1 by the autophagy pathway. Proceedings of the National Academy of Sciences of the United States of America *109*, 15942-15946.

Diaz-Pendon, J.A., Li, F., Li, W.X., and Ding, S.W. (2007). Suppression of antiviral silencing by cucumber mosaic virus 2b protein in Arabidopsis is associated with drastically reduced accumulation of three classes of viral small interfering RNAs. The Plant cell *19*, 2053-2063.

Donaire, L., Barajas, D., Martinez-Garcia, B., Martinez-Priego, L., Pagan, I., and Llave, C. (2008). Structural and genetic requirements for the biogenesis of tobacco rattle virus-derived small interfering RNAs. Journal of virology *82*, 5167-5177.

El-Shami, M., Pontier, D., Lahmy, S., Braun, L., Picart, C., Vega, D., Hakimi, M.A., Jacobsen, S.E., Cooke, R., and Lagrange, T. (2007). Reiterated WG/GW motifs form functionally and evolutionarily conserved ARGONAUTE-binding platforms in RNAi-related components. Genes & development *21*, 2539-2544.

Fahlgren, N., Howell, M.D., Kasschau, K.D., Chapman, E.J., Sullivan, C.M., Cumbie, J.S., Givan, S.A., Law, T.F., Grant, S.R., Dangl, J.L.*, et al.* (2007). High-throughput

sequencing of Arabidopsis microRNAs: evidence for frequent birth and death of MIRNA genes. PloS one *2*, e219.

Felix, G., Duran, J.D., Volko, S., and Boller, T. (1999). Plants have a sensitive perception system for the most conserved domain of bacterial flagellin. The Plant journal : for cell and molecular biology *18*, 265-276.

Finnegan, E.J., Margis, R., and Waterhouse, P.M. (2003). Posttranscriptional gene silencing is not compromised in the Arabidopsis CARPEL FACTORY (DICER-LIKE1) mutant, a homolog of Dicer-1 from Drosophila. Current biology : CB *13*, 236-240.

Garcia-Ruiz, H., A. Takeda, E. J. Chapman, C. M. Sullivan, N. Fahlgren, K. J. Brempelis, and J. C. Carrington. 2010. "Arabidopsis RNA-dependent RNA polymerases and dicer-like proteins in antiviral defense and small interfering RNA biogenesis during Turnip Mosaic Virus infection." *Plant Cell* 22 (2):481-96.

Giner, A., Lakatos, L., García-Chapa, M., López-Moya, JJ., and Burgyán, J. (2010). Viral protein inhibits RISC activity by argonaute binding through conserved GW/WG motifs. PLoS Pathog. 15, e1000996.

Gómez-Gómez, L., Felix, G., and Boller, T. (1999). A single locus determines sensitivity to bacterial flagellin in *Arabidopsis thaliana*. Plant J. 18, 277-84.

Gómez-Gómez, L., Boller, T. (2000). FLS2: an LRR receptor-like kinase involved in the perception of the bacterial elicitor flagellin in Arabidopsis. Mol Cell. 5, 1003-11.

Grefen, C., N. Donald, K. Hashimoto, J. Kudla, K. Schumacher, and M. R. Blatt. 2010. "A ubiquitin-10 promoter-based vector set for fluorescent protein tagging facilitates temporal stability and native protein distribution in transient and stable expression studies." *Plant J* 64 (2):355-65.

Guo, M., Chancey, S.T., Tian, F., Ge, Z., Jamir, Y., and Alfano, J.R. (2005). *Pseudomonas syringae* type III chaperones ShcO1, ShcS1, and ShcS2 facilitate

translocation of their cognate effectors and can substitute for each other in the secretion of HopO1-1. Journal of bacteriology *187*, 4257-4269.

Halter, T., and Navarro, L. (2015). Multilayer and interconnected post-transcriptional and co-transcriptional control of plant NLRs. Current opinion in plant biology *26*, 127-134.

Hamilton, A.J., and Baulcombe, DC. (1999). A species of small antisense RNA in posttranscriptional gene silencing in plants. Science *286*, 950-952.

Harvey, J.J., Lewsey, M.G., Patel, K., Westwood, J., Heimstadt, S., Carr, J.P., and Baulcombe, D.C. (2011). An antiviral defense role of AGO2 in plants. PloS one *6*, e14639.

Hauck, P., Thilmony, R., and He SY. (2003). A *Pseudomonas syringae* type III effector suppresses cell wall-based extracellular defense in susceptible Arabidopsis plants. (2003). Proc Natl Acad Sci U S A. *100*, 8577-82.

Havecker, E. R., L. M. Wallbridge, T. J. Hardcastle, M. S. Bush, K. A. Kelly, R. M. Dunn, F. Schwach, J. H. Doonan, and D. C. Baulcombe. 2010. "The Arabidopsis RNA-directed DNA methylation argonautes functionally diverge based on their expression and interaction with target loci." *Plant Cell* 22 (2):321-34.

Henderson, I. R., X. Zhang, C. Lu, L. Johnson, B. C. Meyers, P. J. Green, and S. E. Jacobsen. 2006. "Dissecting Arabidopsis thaliana DICER function in small RNA processing, gene silencing and DNA methylation patterning." *Nat Genet* 38 (6):721-5.

Hong, J.K., Kang, S.R., Kim, Y.H., Yoon, D.J., Kim, D.H., Kim, H.J., Sung, C.H., Kang, H.S., Choi, C.W., Kim, S.H., *et al*. (2013). Hydrogen Peroxide- and Nitric Oxide-mediated Disease Control of Bacterial Wilt in Tomato Plants. The plant pathology journal *29*, 386-396.

House, B. L., M. W. Mortimer, and M. L. Kahn. 2004. "New recombination methods for Sinorhizobium meliloti genetics." *Appl Environ Microbiol* 70 (5):2806-15.

Ivanov, K., Eskelin, K., Bašić, M; De, S., Lõhmus, A., Varjosalo, M., and Mäkinen, K. (2016). Molecular insights into the function of the viral RNA silencing suppressor HCpro. Plant Journal *85*, 30-45.

Jaubert, M., Bhattacharjee, S., Mello, A.F., Perry, K.L., and Moffett, P. (2011). ARGONAUTE2 mediates RNA-silencing antiviral defenses against Potato virus X in Arabidopsis. Plant physiology *156*, 1556-1564.

Ji, L.H., and Ding, S.W. (2001). The suppressor of transgene RNA silencing encoded by Cucumber mosaic virus interferes with salicylic acid-mediated virus resistance. Molecular plant-microbe interactions: MPMI *14*, 715-724.

Jones, J.D., and Dangl, J.L. (2006). The plant immune system. Nature *444*, 323-329.

Jones, J.D., Vance, R.E., and Dangl, J.L. (2016). Intracellular innate immune surveillance devices in plants and animals. Science *354*.

Karran, R.A., and Sanfacon, H. (2014). Tomato ringspot virus coat protein binds to ARGONAUTE 1 and suppresses the translation repression of a reporter gene. Molecular plant-microbe interactions: MPMI *27*, 933-943.

Katiyar-Agarwal, S., Morgan, R., Dahlbeck, D., Borsani, O., Villegas, A., Jr., Zhu, J.K., Staskawicz, B.J., and Jin, H. (2006). A pathogen-inducible endogenous siRNA in plant immunity. Proceedings of the National Academy of Sciences of the United States of America *103*, 18002-18007.

Katiyar-Agarwal, S., Gao, S., Vivian-Smith, A., and Jin, H. (2007). A novel class of bacteria-induced small RNAs in Arabidopsis. Genes & development *21*, 3123-3134.

King, E. O., M. K. Ward, and D. E. Raney. 1954. "Two simple media for the demonstration of pyocyanin and fluorescin." *J Lab Clin Med* 44 (2):301-7.

Kurihara, Y., and Watanabe, Y. (2004). Arabidopsis micro-RNA biogenesis through Dicer-like 1 protein functions. Proceedings of the National Academy of Sciences of the United States of America *101*, 12753-12758.

La Camera, S., C. Balague, C. Gobel, P. Geoffroy, M. Legrand, I. Feussner, D. Roby, and T. Heitz. 2009. "The Arabidopsis patatin-like protein 2 (PLP2) plays an essential role in cell death execution and differentially affects biosynthesis of oxylipins and resistance to pathogens." *Mol Plant Microbe Interact* 22 (4):469-81.

Li, X., Lin, H., Zhang, W., Zou, Y., Zhang, J., Tang, X., and Zhou, J.M. (2005). Flagellin induces innate immunity in nonhost interactions that is suppressed by *Pseudomonas syringae* effectors. Proceedings of the National Academy of Sciences of the United States of America *102*, 12990-12995.

Li, Y., Zhang, Q., Zhang, J., Wu, L., Qi, Y., and Zhou, J.M. (2010). Identification of microRNAs involved in pathogen-associated molecular pattern-triggered plant innate immunity. Plant physiology *152*, 2222-2231.

Li, L., Yu, Y., Zhou, Z., and Zhou, J.M. (2016). Plant pattern-recognition receptors controlling innate immunity. Sci China Life Sci. 59, 1350.

Llave, C., Kasschau, K.D., Rector, M.A., and Carrington, J.C. (2002). Endogenous and silencing-associated small RNAs in plants. The Plant cell *14*, 1605-1619.

Lobbes, D., Rallapalli, G., Schmidt, DD., Martin, C., Clarke, J. (2006). SERRATE: a new player on the plant microRNA scene. EMBO Rep. *7*, 1052-1058.

Misas-Villamil, J.C., Kolodziejek, I., and van der Hoorn, R.A. (2011). Pseudomonas syringae colonizes distant tissues in Nicotiana benthamiana through xylem vessels. The Plant journal: for cell and molecular biology *67*, 774-782.

Morel, J.B., Godon, C., Mourrain, P., Beclin, C., Boutet, S., Feuerbach, F., Proux, F., and Vaucheret, H. (2002). Fertile hypomorphic ARGONAUTE (ago1) mutants

impaired in post-transcriptional gene silencing and virus resistance. The Plant cell *14*, 629-639.

Mourrain, P., Beclin, C., Elmayan, T., Feuerbach, F., Godon, C., Morel, J.B., Jouette, D., Lacombe, A.M., Nikic, S., Picault, N.*, et al.* (2000). Arabidopsis SGS2 and SGS3 genes are required for posttranscriptional gene silencing and natural virus resistance. Cell *101*, 533-542.

Navarro, L., Zipfel, C., Rowland, O., Keller, I., Robatzek, S., Boller, T., and Jones, J.D. (2004). The transcriptional innate immune response to flg22. Interplay and overlap with Avr gene-dependent defense responses and bacterial pathogenesis. Plant physiology *135*, 1113-1128.

Navarro, L., Dunoyer, P., Jay, F., Arnold, B., Dharmasiri, N., Estelle, M., Voinnet, O., and Jones, J.D. (2006). A plant miRNA contributes to antibacterial resistance by repressing auxin signaling. Science *312*, 436-439.

Navarro, L., Jay, F., Nomura, K., He, S.Y., and Voinnet, O. (2008). Suppression of the microRNA pathway by bacterial effector proteins. Science *321*, 964-967.

Oldroyd, G.E., and Staskawicz, B.J. (1998). Genetically engineered broad-spectrum disease resistance in tomato. Proceedings of the National Academy of Sciences of the United States of America *95*, 10300-10305.

Palatnik, J.F., Allen, E., Wu, X., Schommer, C., Schwab, R., Carrington, J.C., and Weigel, D. (2003). Control of leaf morphogenesis by microRNAs. Nature *425*, 257-263.

Park, W., Li, J., Song, R., Messing, J., and Chen, X. (2002). CARPEL FACTORY, a Dicer homolog, and HEN1, a novel protein, act in microRNA metabolism in Arabidopsis thaliana. Current biology: CB *12*, 1484-1495.

Poulsen, C., Vaucheret, H., Brodersen, P. (2013). Lessons on RNA silencing mechanisms in plants from eukaryotic argonaute structures. Plant Cell 25, 22-37.

Pruss, G., Lawrence, C.B., Bass, T., Li, Q.Q., Bowman, L.H., and Vance, V. (2004). The potyviral suppressor of RNA silencing confers enhanced resistance to multiple pathogens. Virology *320*, 107-120.

Pumplin, N., and Voinnet, O. (2013). RNA silencing suppression by plant pathogens: defence, counter-defence and counter-counter-defence. Nature reviews. Microbiology *11*, 745-760.

Qiao, Y., Shi, J., Zhai, Y., Hou, Y., and Ma, W. (2015). Phytophthora effector targets a novel component of small RNA pathway in plants to promote infection. Proceedings of the National Academy of Sciences of the United States of America *112*, 5850-5855.

Rajagopalan, R., Vaucheret, H., Trejo, J., and Bartel, D.P. (2006). A diverse and evolutionarily fluid set of microRNAs in Arabidopsis thaliana. Genes Dev. *20*: 3407-3425.

Rate, D.N., Cuenca, J.V., Bowman, G.R., Guttman, D.S., and Greenberg, J.T. (1999). The gain-of-function Arabidopsis acd6 mutant reveals novel regulation and function of the salicylic acid signaling pathway in controlling cell death, defenses, and cell growth. The Plant cell *11*, 1695-1708.

Rhoades, M.W., Reinhart, B.J., Lim, L.P., Burge, C.B., Bartel, B., and Bartel, D.P. (2002). Prediction of plant microRNA targets. Cell *110*, 513-520.

Staiger, D., Korneli, C., Lummer, M., and Navarro, L. (2013). Emerging role for RNA-based regulation in plant immunity. New Phytol. *197*, 394-404.

Tao, Y., Yuan, F., Leister, R.T., Ausubel, F.M., and Katagiri, F. (2000). Mutational analysis of the Arabidopsis nucleotide binding site-leucine-rich repeat resistance gene RPS2. The Plant cell *12*, 2541-2554.

Till, S., Lejeune, E., Thermann, R., Bortfeld, M., Hothorn, M., Enderle, D., Heinrich, C., Hentze, M.W., and Ladurner, A.G. (2007). A conserved motif in Argonaute-interacting proteins mediates functional interactions through the Argonaute PIWI domain. Nature structural & molecular biology *14*, 897-903.

Thomas, W.J., Thireault, C.A., Kimbrel, J.A., and Chang, J.H. (2009) Recombineering and stable integration of the Pseudomonas syringae pv. syringae 61 hrp/hrc cluster into the genome of the soil bacterium Pseudomonas fluorescens Pf0-1. Plant J. *60*, 919-928.

Torres, M.A., Jones, J.D., and Dangl, J.L. (2006). Reactive oxygen species signaling in response to pathogens. Plant Physiol. 141, 373-378.

Tsuda, K., and Katagiri, F. (2010). Comparing signaling mechanisms engaged in pattern-triggered and effector-triggered immunity. Current opinion in plant biology *13*, 459-465.

van der Biezen, E.A., and Jones, J.D. (1998). The NB-ARC domain: a novel signalling motif shared by plant resistance gene products and regulators of cell death in animals. Current biology: CB *8*, R226-227.

Varallyay, E., Valoczi, A., Agyi, A., Burgyan, J., and Havelda, Z. (2010). Plant virus-mediated induction of miR168 is associated with repression of ARGONAUTE1 accumulation. The EMBO journal *29*, 3507-3519.

Varkonyi-Gasic E., Wu R., Wood M., Walton E.F. and Hellens R.P. (2007). Protocol: a highly sensitive RT-PCR method for detection and quantification of microRNAs. Plant Methods. 12;3:12.

Vaucheret, H. (2008). Plant ARGONAUTES. Trends Plant Sci. *13*, 350-358.

Vaucheret, H., Vazquez, F., Crete, P., and Bartel, D.P. (2004). The action of ARGONAUTE1 in the miRNA pathway and its regulation by the miRNA pathway are crucial for plant development. Genes and development *18*, 1187-1197.

Weiberg, A., Bellinger, M., and Jin, H. (2015). Conversations between kingdoms: small RNAs. Current opinion in biotechnology *32*, 207-215.

Windgassen, M., A. Urban, and K. E. Jaeger. 2000. "Rapid gene inactivation in Pseudomonas aeruginosa." *FEMS Microbiol Lett* 193 (2):201-5.

Wong, J., Gao, L., Yang, Y., Zhai, J., Arikit, S., Yu, Y., Duan, S., Chan, V., Xiong, Q., Yan, J.*, et al.* (2014). Roles of small RNAs in soybean defense against Phytophthora sojae infection. The Plant journal: for cell and molecular biology *79*, 928-940.

Xie, Z., Kasschau, K.D., and Carrington, J.C. (2003). Negative feedback regulation of Dicer-Like1 in Arabidopsis by microRNA-guided mRNA degradation. Curr Biol. *13*, 784-789.

Xie, Z., Johansen, L.K., Gustafson, A.M., Kasschau, K.D., Lellis, A.D., Zilberman, D., Jacobsen, S.E., and Carrington, J.C. (2004). Genetic and functional diversification of small RNA pathways in plants. PLoS biology *2*, E104.

Yi, H., and Richards, E.J. (2007). A cluster of disease resistance genes in Arabidopsis is coordinately regulated by transcriptional activation and RNA silencing. Plant Cell. *19*, 2929-2939.

Yu, A., Lepere, G., Jay, F., Wang, J., Bapaume, L., Wang, Y., Abraham, A.L., Penterman, J., Fischer, R.L., Voinnet, O.*, et al.* (2013). Dynamics and biological relevance of DNA demethylation in Arabidopsis antibacterial defense. Proceedings of the National Academy of Sciences of the United States of America *110*, 2389-2394.

Zhang, Y., Goritschnig, S., Dong, X., and Li, X. (2003). A gain-of-function mutation in a plant disease resistance gene leads to constitutive activation of downstream signal transduction pathways in suppressor of *npr1-1*, constitutive 1. The Plant cell *15*, 2636-2646.

Zhang, Y., Dorey, S., Swiderski, M., and Jones, J.D. (2004). Expression of RPS4 in tobacco induces an AvrRps4-independent HR that requires EDS1, SGT1 and HSP90. The Plant journal : for cell and molecular biology *40*, 213-224.

Zhang, X., Yuan, Y.R., Pei, Y., Lin, S.S., Tuschl, T., Patel, D.J., and Chua, N.H. (2006). Cucumber mosaic virus-encoded 2b suppressor inhibits Arabidopsis Argonaute1 cleavage activity to counter plant defense. Genes & development *20*, 3255-3268.

Zhang, JF., Yuan, LJ., Shao, Y., Du, W., Yan, DW., and Lu, YT. (2008). The disturbance of small RNA pathways enhanced abscisic acid response and multiple stress responses in Arabidopsis. Plant Cell Environ. 31, 562-74.

Zhang, X., Zhao, H., Gao, S., Wang, W.C., Katiyar-Agarwal, S., Huang, H.D., Raikhel, N., and Jin, H. (2011). Arabidopsis Argonaute 2 regulates innate immunity via miRNA393(*)-mediated silencing of a Golgi-localized SNARE gene, MEMB12. Mol Cell. *42*, 356-366.

Zhang, Z., A. Lenk, M. X. Andersson, T. Gjetting, C. Pedersen, M. E. Nielsen, M. A. Newman, B. H. Hou, S. C. Somerville, and H. Thordal-Christensen. 2008. "A lesion-mimic syntaxin double mutant in Arabidopsis reveals novel complexity of pathogen defense signaling." *Mol Plant* 1 (3):510-27.

Zhang, Z., Wu, Y., Gao, M., Zhang, J., Kong, Q., Liu, Y., Ba, H., Zhou, J., and Zhang, Y. (2012). Disruption of PAMP-induced MAP kinase cascade by a *Pseudomonas syringae* effector activates plant immunity mediated by the NB-LRR protein SUMM2. Cell Host Microbe. *11*, 253-263.

Zipfel, C., Robatzek, S., Navarro, L., Oakeley, E.J., Jones, J.D., Felix, G., and Boller, T. (2004). Bacterial disease resistance in Arabidopsis through flagellin perception. Nature *428*, 764-767.

Zipfel, C., Kunze, G., Chinchilla, D., Caniard, A., Jones, JD., Boller, T., Felix, G. (2006). Perception of the bacterial PAMP EF-Tu by the receptor EFR restricts Agrobacterium-mediated transformation. *Cell* 125, 749-60.

FIGURE LEGENDS

Figure 1. The growth defect of the *hopT1-1*-deleted strain of *Pto* DC3000 is specifically rescued in Arabidopsis miRNA-defective mutants

Five-week-old Col-0 Arabidopsis (WT) plants and indicated genotypes were dip-inoculated with bacterial strain *Pto* DC3000 (*Pto*) (blue dots) and *Pto ΔhopT1-1* (green dots) or *Pto ΔhopC1* (orange dots) at a concentration of 10^8 cfu/mL. At three days post-inoculation, leaves from three plants were collected and bacterial titers were further monitored. Each dot represents number of bacteria as log (cfu per cm^2) and mean (n=8 or 16) is represented as horizontal line. Statistical significance was assessed using the ANOVA test (n.s.: p-value>0.05; *: p-value<0.01; **: p-value<0.001; ***: p-value<0.0001; ****: p-value<0.00001). Similar results were obtained in two to three independent experiments (as shown in Figure S1). **(A)** The growth of *hopT1-1* deleted bacterial strain (*Pto ΔhopT1-1)* is partially impaired in WT plants in comparison to the wild type *Pto* DC3000 strain. In three different alleles of *ago1* mutants, namely *ago1-25*, *ago1-26* and *ago1-27*, the growth of the *Pto ΔhopT1-1* strain is similar to the growth of the *Pto* DC3000 strain (left panel). The *Pto ΔhopC1* strain shows similar growth defect in WT plants and in *ago1-27* mutant as

compared to the titer of *Pto* DC3000 strain (right panel). **(B)** The growth defect of the *Pto ΔhopT1-1* strain is not rescued in other *ago* mutants: *ago2-1* (left panel), *ago4-2* and *ago4-3* (right panel). **(C)** miRNA biogenesis mutants, *se-1* and *dcl1-11*, exhibit a complete rescue in the growth defect of the *Pto ΔhopT1-1* strain, similar to *ago1* mutants (left panel). The growth defect of the *Pto ΔhopC1* strain remains unaffected in *se-1* mutant when compared to WT plants (right panel). **(D)** The growth defect of the *Pto ΔhopT1-1* strain, when compared to the *Pto* DC3000, is not rescued in siRNA biogenesis mutants: *rdr1-1 rdr2-1 rdr6-15*, *dcl2-1 dcl4-2* and *sgs3-1*.

Figure 2. HopT1-1 interacts with AGO1 in a GW-dependent manner

(A) Schematic representation of HopT1-1 and of HopT1-1m3 protein sequences with the position of the WT GW motifs (GW) and the mutated GW motifs (GF), respectively. **(B)** To determine whether HopT1-1 interacts *in vivo* with AGO1, BiFC assay was performed in *N. benthamiana*. Four-week-old *N. benthamiana* were co-infiltrated with combination of *Agrobacterium tumefaciens* strains carrying different constructs fused with N-ter or C-ter part of YFP. Interaction of NYFP-AGO1 with CYFP-HopT1-1 (left-bottom) or with CYFP-HopT1-1m3 (right-bottom) was tested. As negative controls, NYFP-AGO1 was co-infiltrated with CYFP-HopC1 (left-top) and NYFP-SDE3 was co-infiltrated with CYFP-HopT1-1 (right-top). YFP fluorescence was visualized by confocal microscopy three days post-infiltration and quantification of the fluorescence signal for each picture taken (n=10) was performed using ImageJ software. Each dot represents the intensity of fluorescence signal resulting in the interaction of each pair of combination as indicated in the dot plot. Two biological replicates are presented and the mean is represented as the horizontal line. Statistical significance was assessed using the ANOVA test (n.s.: p-value>0.05; ****:

p-value<0.0001). **(C)** Similar results were obtained when the same constructs in (B) were fused with the reversed NYFP and CYFP tags. Two biological replicates are presented for these combinations in the dot plot. **(D)** Subcellular localization of GFP, GFP-AGO1, GFP-HopT1-1 and GFP-HopT1-1m3 proteins transiently expressed in *N. benthamiana* leaves. Four-week-old leaves of *N. benthamiana* were infiltrated with *Agrobacterium tumefaciens* strain expressing the indicated proteins. Multiple sections of leaves were visualized at 2 dpi using confocal microscope. Representative picture of the whole set of leaf patches analysed (n=12) is depicted. **(E)** To assess which GW motif/s of HopT1-1 is/are required for interaction with AGO1, synthetic biotinylated peptides containing the WT (GW) or the mutated version (GF) of each GW motifs of HopT1-1 were mobilized on streptavidin magnetic beads. Specific peptide-loaded beads were further incubated with total protein extracted from Flag-AGO1 inflorescence. The presence of Flag-AGO1 in the total extract protein (input) and bound to the beads was assessed by immunoblotting. The peptides GW2 and GW3, but not GW1, can interact with Flag-AGO1. This interaction was partially or completely impaired in presence of GF2 and GF3, respectively.

Figure 3. HopT1-1 suppresses AGO1-mediated miRNA function in a GW-dependent manner

(A) Representative pictures of a leaf of six-week-old *SUC2$_{pro}$:amiR-SUL* plants (WT1) along with independent T2 transgenic *SUC2$_{pro}$:amiR-SUL* plants constitutively expressing HopT1-1. White bar represents 0.5 cm. **(B)** Same as (A), but pictures of five-week-old *SUC2$_{pro}$:amiR-SUL* plants (WT2) along with independent T2 transgenic *SUC2$_{pro}$:amiR-SUL* plants constitutively expressing HopT1-1m3. White bar represents 0.5 cm. Plants were grown in parallel and in the same growth conditions

to the plants depicted in (A) but were collected one week before. For the molecular analysis, leaves from six plants were collected and pooled from HopT1-1 and HopT1-1m3 expressing transgenic lines along with WT1 and WT2, respectively. **(C)** Relative mRNA accumulation levels of *SUL* and multiple endogenous miRNA target transcripts in the HopT1-1 expressing transgenic lines in comparison to WT1 were monitored by RT-qPCR analysis. *Ubiquitin* was used as a control and the error bars represent the standard deviation from three technical replicates. **(D)** Same as (C) but using the HopT1-1m3 expressing transgenic lines in comparison to WT2. **(E)** Protein accumulation level of some endogenous miRNA targets AGO1, DCL1 and AGO2, was assessed by immunoblotting. Similarly, SUL protein accumulation level was also monitored. Protein accumulation level of AGO4 was used as an internal control, as this silencing factor is not targeted by any miRNA. UGP protein accumulation level was used as loading control.

Figure 4. HopT1-1 dampens PTI in a GW-dependent manner and its presence mimics the impaired PTI responses observed in *ago1* mutants

(A) Flg22-induced ROS production assay was performed in leaf discs from DEX-treated samples. Five-week-old Col-0 Arabidopsis (WT) plants and T2 transgenic lines expressing Myc-HopT1-1 or Myc-HopT1-1m3 under the dexamethasone (DEX) inducible promoter (DEX_{pro}:*HopT1-1* and DEX_{pro}:*HopT1-1m3*, respectively) were sprayed every 24 hours for three consecutive days with 30 µM of DEX. For each condition, leaves from three plants were subsequently used to prepare leaf discs. Luminescence (Relative Light Unit; RLU) was measured over flg22-elicitated time-course for each technical replicate. Each dot represents the total amount of RLU produced during the flg22-elicitated time-course and the mean is represented as

horizontal bar in the dot plot. Plants expressing Myc-HopT1-1 exhibit significant reduction in flg22-induced ROS production compared with WT plants or plants expressing Myc-HopT1-1m3. **(B)** Detection of H_2O_2 production in the leaves of WT plants 24 hours after infiltration with the EtHAn strain alone (EtHAn) or with EtHAn strain carrying a plasmid encoding for HopT1-1 or HopT1-1m3, respectively (left panel). Around 20-30 pictures were taken for each condition and leaves from three plants were treated to clear the chlorophyll pigments and were further incubated with DAB staining buffer to detect the presence of H_2O_2. In each condition, absolute value of DAB staining was quantified using ImageJ software and presented as a dot plot (right panel). **(C)** Presence of callose deposits was detected 7 hours after infiltration of WT plants with the EtHAn strains used in (B). For each condition, leaves from three plants were collected and stained with aniline blue to detect the presence of callose deposits. The amount of callose deposits was measured using ImageJ software and presented as a dot blot. **(D)** As in (A) but in WT and *ago1* mutant alleles, *ago1-25*, *ago1-26* and *ago1-27*. **(E)** As in (A) but in WT, *ago1-27*, *dcl1-11* and *se-1* mutants. **(F)** Same analysis as in (B) but in mock or in EtHAn-infiltrated plants on WT plants *versus ago1-27* mutant. **(G)** Same analysis as in (C) but in mock or in EtHAn-infiltrated plants on WT plants *versus ago1-27* mutant.

Note: For all the above experiments, statistical significance were assessed using the ANOVA test (n.s.: p-value>0.05; *: p-value<0.01; **: p-value<0.001; ***: p-value<0.0001; ****: p-value<0.00001). All the results shown in different panels of the figure were obtained in at least two or three independent experiments represented in the dot plots as Rep1, Rep2 and Rep3 respectively.

Figure 5. The BSR activity of HopT1-1 triggers a potent ETI response that is compromised at high temperature regime

(A) Representative pictures of six-week-old *SUC2$_{pro}$:amiR-SUL* plants (WT1) along with independent T2 transgenic *SUC2$_{pro}$:amiR-SUL* plants expressing HopT1-1. The HopT1-1 expressing plants shows dwarf phenotype as compared to WT1 plants when grown at 23°C. **(B)** Same as (A) but pictures of five-week-old *SUC2$_{pro}$:amiR-SUL* plants (WT2) along with independent T2 transgenic *SUC2$_{pro}$:amiR-SUL* plants expressing HopT1-1m3. No distinct phenotype was observed for these plants when compared to WT2. **(C)** Relative mRNA levels of *PR1* in HopT1-1 and HopT1-1m3 expressing plants compared with WT1 and WT2, respectively, was performed by RT-qPCR analysis. Similarly, relative mRNA levels of other SA-dependent marker genes like *PR2*, *PR5* and *ICS1* were also monitored. *Ubiquitin* was used as a control and the error bars represent the standard deviation from three technical repeats. Higher transcript levels were obtained for the plants expressing HopT1-1 as compared to WT and HopT1-1m3. **(D)** Same as in (C) but, relative mRNA accumulation level of cell death (*ALD1*) and senescence marker (*WRKY75*) was monitored. **(E)** Wild-type *SUC2$_{pro}$:amiR-SUL* plants and transgenic *SUC2$_{pro}$:amiR-SUL* plants expressing HopT1-1 were grown in parallel at 23°C and at 28°C. Representative pictures of the plants growing at 28°C are presented.

Figure 6. Stable expression of an *AGO1* transgene that is refractory to miR168 is sufficient to trigger an ETI-like response

(A) Upper panel: Schematic representation of the *AGO1$_{pro}$:4m-AGO1* (4m-AGO1) transgene that is refractory to miR168 action under the control of the native *AGO1*

promoter. Four silent mutations (in red) were introduced (*4m-AGO1*) in the miR168 target site of *AGO1*. Bottom panel: Schematic representation of the hypothesis by which over-accumulation of the miR168-refractory version of *AGO1* may trigger an ETI-like response. **(B)** *AGO1*$_{pro}$*:4m-AGO1* construct was transformed in WT plants or in *pad4 sid2* mutant. Primary transformants show a WT-like or a mir-AGO1 phenotype in both WT and *pad4 sid2* mutant. Leaves from a pool of six-week-old primary transformants exhibiting the same phenotype were collected for molecular analysis. Relative *AGO1* mRNA levels in WT plants or in *4m-AGO1* transgenic plants, were monitored by RT-qPCR analysis using *Ubiquitin* as control. The error bars represent the standard deviation from three technical replicates. Protein accumulation of AGO1 was assessed by immunoblotting. Coomassie staining was used as a loading control. **(C)** To detect the presence of cell death, trypan blue staining was performed on leaves of WT-like and mir-AGO1 plants. Representative pictures are depicted along with the number of pictures showing the same phenotype as compared to the total number of pictures taken. Plants with mir-AGO1 phenotype exhibit constitutive cell death within and around Arabidopsis leaf vasculature. **(D)** Relative mRNA levels of *PR1*, *PR2*, *PR5* and *ICS1/SID2* mRNA were monitored by RT-qPCR analysis from the same samples used in (B). **(E)** Same as in (D) but *ALD1* and *WRKY75* mRNA levels were monitored.

Note: All the results shown in the different panels of the figure were obtained in two independent experiments.

Figure 7. Hypothetical model for HopT1-1-induced molecular effects in host cells.

(A) Representation of Negative Regulator of PTI (NRP)-, and AGO1-transcripts that

are targeted by miRNAs in the absence of HopT1-1. MiRNA species that target NRP transcripts (in blue) and miR168 species (in orange) are loaded in AGO1. **(B)** HopT1-1 interacts with AGO1 in a GW-dependent manner to suppress AGO1 silencing activity. In the model, we propose possible mechanisms by which HopT1-1 might suppress PTI and trigger ETI. In the presence of HopT1-1, AGO1 is no longer able to trigger silencing of NRP mRNAs, which results in an enhanced production of NRPs, such as *ARF17* that can contribute to PTI suppression (left panel). Similarly, in the presence of HopT1-1, AGO1 is no longer able to silence its own transcript, which results in AGO1 protein hyper-accumulation. Perturbation of miR168-directed control of AGO1 homeostasis might be sensed by yet-unknown NLR proteins that are there to guard the integrity of AGO1 homeostasis. HopT1-1-induced disruption of AGO1 homeostasis results in a *PAD4-/NDR1-/SID2*-dependent immune response that culminates in SA-dependent signalling and ETI (right panel). Question marks depict hypothetical molecular effects that have not been experimentally validated. Indeed, we still do not know whether or not HopT1-1 could interfere with the loading of miRNAs in AGO1 or whether NLRs can directly bind to AGO1.

TABLE LEGEND

Donor	Acceptor	τ	sem[(a)]	Δ[(b)]	N[(c)]	E[(d)]	p-value
CFP-AGO1	-	2.858	0.029	-	79	-	-
CFP-AGO1	HopT1-1-YFP	2.516	0.032	342	60	11.2	$2E^{-10}$
CFP-AGO1	HopT1-m3-YFP	2.904	0.034	46	50	1.61	0.32
CFP-AGO1	HopT1-1-HA	2.8	0.028	28	34	0.99	0.65

Table 1. FRET-FLIM measurements showing that HopT1-1, but not HopT1-1m3, interacts with AGO1 in the cytoplasm of plant cells.

Mean lifetime, τ, in ns. [(a)] For each cell analyzed, average fluorescence decay profiles measured in the cytoplasm were plotted and fitted with exponential function using a non-linear square estimation procedure and the mean lifetime was calculated according to $\tau=\sum \langle_i \tau_i^2 / \sum \langle_i \tau_i$ with $I(t) = \sum \alpha_i e^{-t/\tau i}$, standard error of the mean, [(b)] $\Delta t=\tau_D-\tau_{DA}$ (in ps), [(c)] total number of measured cell cytoplasm, and [(d)] % FRET efficiency: $E = 1 – (\tau_{DA}/\tau_D)$. p-value of the difference between the donor lifetimes in the presence and in the absence of acceptor (Student's *t* test).

ACKNOWLEDGMENTS

We thank O. Voinnet for DCL1 and AGO2 antibodies, D. Weigel for the *SUC2*$_{pro}$:*amiR-SUL* line, H. Vaucheret for the *4m-AGO1* plasmid, P. Genschik for the CFP-AGO1 construct, J. Chang for the EtHAn strain, M. Grant for the *DEX*$_{pro}$*:AvrRPM1* line and and members of the Navarro Lab for critical reading of the manuscript. We are grateful to the PlantAlgae Facility of the IBENS, which received the support under the program "Investissements d'Avenir" ANR-10-Labx-54 MEMOLIFE and ANR-11-IDEX-0001-02 PSL* Research University and of the SESAME Program from the "Région Île-de-France"; the Imaging Facility of IBENS, which received the support of grants from the "Région Île-de-France" (NERF N°2011-45), the "Fondation pour la Recherche Médicale" (N° DGE 20111123023) and the

“Fédération pour la Recherche sur le Cerveau - Rotary International France” (2011) and the TRI-Genotoul platform, which was supported by the “Région Occitanie/Pyrénées-Méditerranée” (PRISM-Project). This work was supported by an European Research Council starting grant (to L.N.), an ATIP-Avenir Grant from the Fondation Bettencourt Schueller (to L.N.), a grant from the National Institutes of Health (to J.R.A.), and support from the Center for Plant Science Innovation at the University of Nebraska (to J.R.A.), by an ANR grant (08-BLAN-0206) and support from the CNRS (to T.L. and D.P.), by an ANR grant (15-CE20-0016-01) and support from the French Laboratory of Excellence ‘TULIP’ (ANR-10-LABX-41; ANR-11-IDEX-0002-02) (to L.D.) and by the “Région Occitanie/Pyrénées-Méditerranée” PRISM-Project (to C.P.).

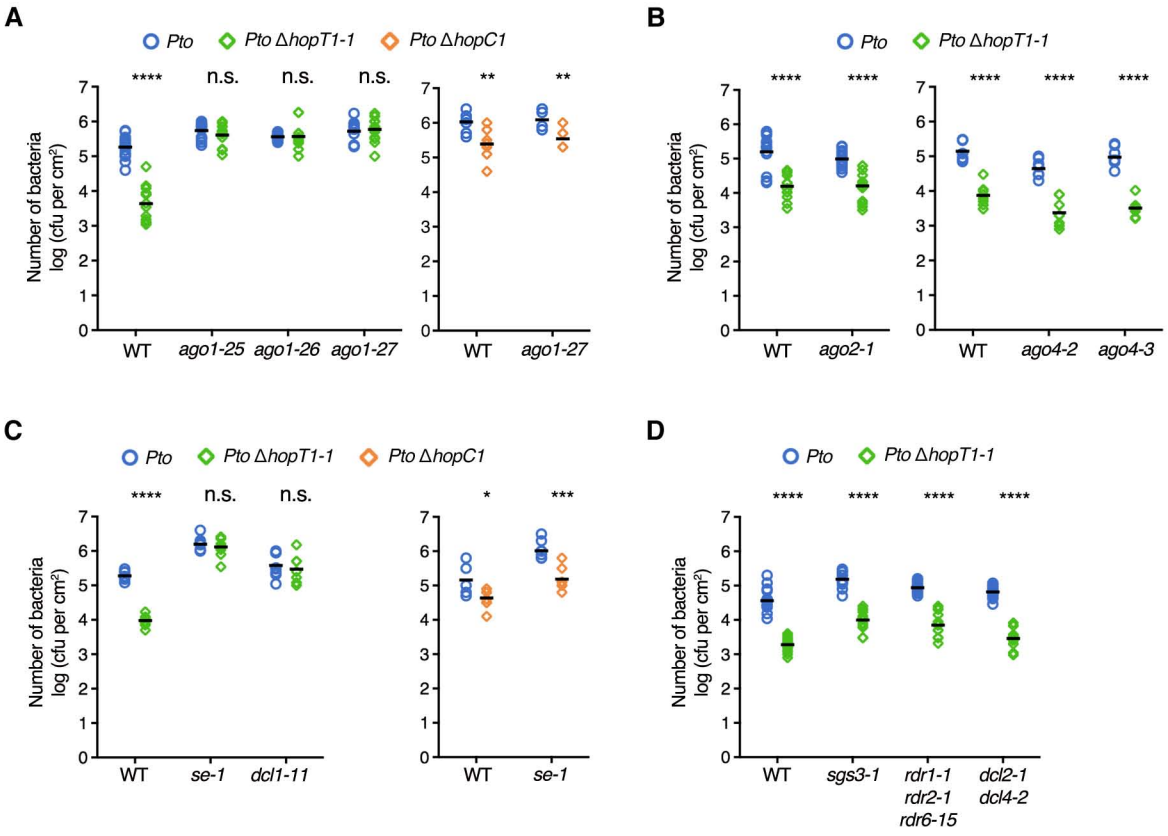

Figure 1. The growth defect of the *hopT1-1*-deleted strain of *Pto* DC3000 is specifically rescued in Arabidopsis miRNA-defective mutants
Five-week-old Col-0 Arabidopsis (WT) plants and indicated genotypes were dip inoculated with bacterial strain *Pto* DC3000 (*Pto*) (blue dots) and *Pto* Δ*hopT1-1* (green dots) or *Pto* Δ*hopC1* (orange dots) at a concentration of 10^8 cfu/mL. At three days post-inoculation, leaves from three plants were collected and bacterial titers were further monitored. Each dot represents number of bacteria as log (cfu per cm^2) and mean (n=8 or 16) is represented as horizontal line. Statistical significance was assessed using the ANOVA test (n.s.: p-value>0.05; *: p-value<0.01; **: p-value<0.001; ***: p-value<0.0001; ****: p-value<0.00001). Similar results were obtained in two to three independent experiments (as shown in Figure S1). **(A)** The growth of *hopT1-1* deleted bacterial strain (*Pto* Δ*hopT1-1*) is partially impaired in WT plants in comparison to the wild type *Pto* DC3000 strain. In three different alleles of *ago1* mutants, namely *ago1-25*, *ago1-26* and *ago1-27*, the growth of the *Pto* Δ*hopT1-1* strain is similar to the growth of the *Pto* DC3000 strain (left panel). The *Pto* Δ*hopC1* strain shows similar growth defect in WT plants and in *ago1-27* mutant as compared to the titer of *Pto* DC3000 strain (right panel). **(B)** The growth defect of the *Pto* Δ*hopT1-1* strain is not rescued in other *ago* mutants: *ago2-1* (left panel), *ago4-2* and *ago4-3* (right panel). **(C)** miRNA biogenesis mutants, *se-1* and *dcl1-11*, exhibit a complete rescue in the growth defect of the *Pto* Δ*hopT1-1* strain, similar to *ago1* mutants (left panel). The growth defect of the *Pto* Δ*hopC1* strain remains unaffected in *se-1* mutant when compared to WT plants (right panel). **(D)** The growth defect of the *Pto* Δ*hopT1-1* strain, when compared to the *Pto* DC3000, is not rescued in siRNA biogenesis mutants: *rdr1-1 rdr2-1 rdr6-15*, *dcl2-1 dcl4-2* and *sgs3-1*.

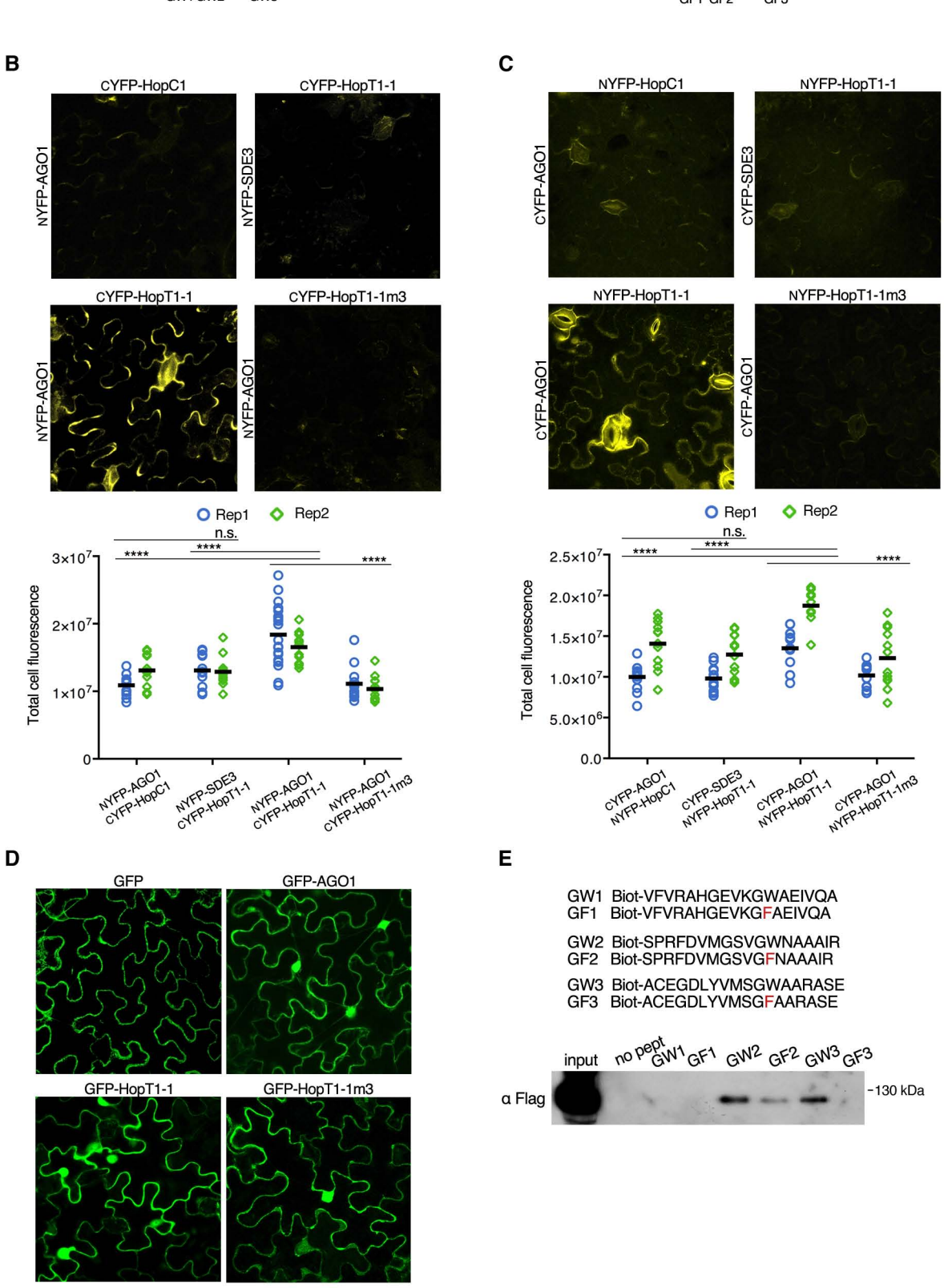

Figure 2. HopT1-1 interacts with AGO1 in a GW-dependent manner

(A) Schematic representation of HopT1-1 and of HopT1-1m3 protein sequences with the position of the WT GW motifs (GW) and the mutated GW motifs (GF), respectively. **(B)** To determine whether HopT1-1 interacts *in vivo* with AGO1, BiFC assay was performed in *N. benthamiana*. Four-week-old *N. benthamiana* were co-infiltrated with combination of *Agrobacterium tumefaciens* strains carrying different constructs fused with N-ter or C-ter part of YFP. Interaction of NYFP-AGO1 with CYFP-HopT1-1 (left-bottom) or with CYFP-HopT1-1m3 (right-bottom) was tested. As negative controls, NYFP-AGO1 co-infiltrated with CYFP-HopC1 (left-top) and NYFP-SDE3 co-infiltrated with CYFP-HopT1-1 (right-top) were used. YFP fluorescence was visualized by confocal microscopy three days post-infiltration and quantification of the fluorescence signal for each picture taken (n=10) was performed using ImageJ software. Each dot represents the intensity of fluorescence signal resulting in the interaction of each pair of combination as indicated in the dot plot. Two biological replicates are presented and the mean is represented as the horizontal line. Statistical significance was assessed using the ANOVA test (n.s.: p-value>0.05; ****: p-value<0.0001). **(C)** Similar results were obtained when the same constructs in (B) were fused with the reversed NYFP and CYFP tags. Two biological replicates are presented for these combinations in the dot plot. **(D)** Subcellular localization of GFP, GFP-AGO1, GFP-HopT1-1 and GFP-HopT1-1m3 proteins transiently expressed in *N. benthamiana* leaves. Four-week-old leaves of *N. benthamiana* were infiltrated with *Agrobacterium tumefaciens* strain expressing the indicated proteins. Multiple sections of leaves were visualized at 2 dpi using confocal microscope. Representative picture of the whole set of leaf patches analysed (n=12) is depicted. **(E)** To assess which GW motif/s of HopT1-1 is/are required for interaction with AGO1, synthetic biotinylated peptides containing the WT (GW) or the mutated version (GF) of each GW motifs of HopT1-1 were mobilized in streptavidin magnetic beads. Specific peptide-loaded beads were further incubated with total protein extracted from Flag-AGO1 inflorescence. The presence of Flag-AGO1 in the total extract protein (input) and bound to the beads was assessed by immunoblotting. The peptides GW2 and GW3, but not GW1, can interact with Flag-AGO1. This interaction was partially or completely impaired in presence of GF2 and GF3, respectively.

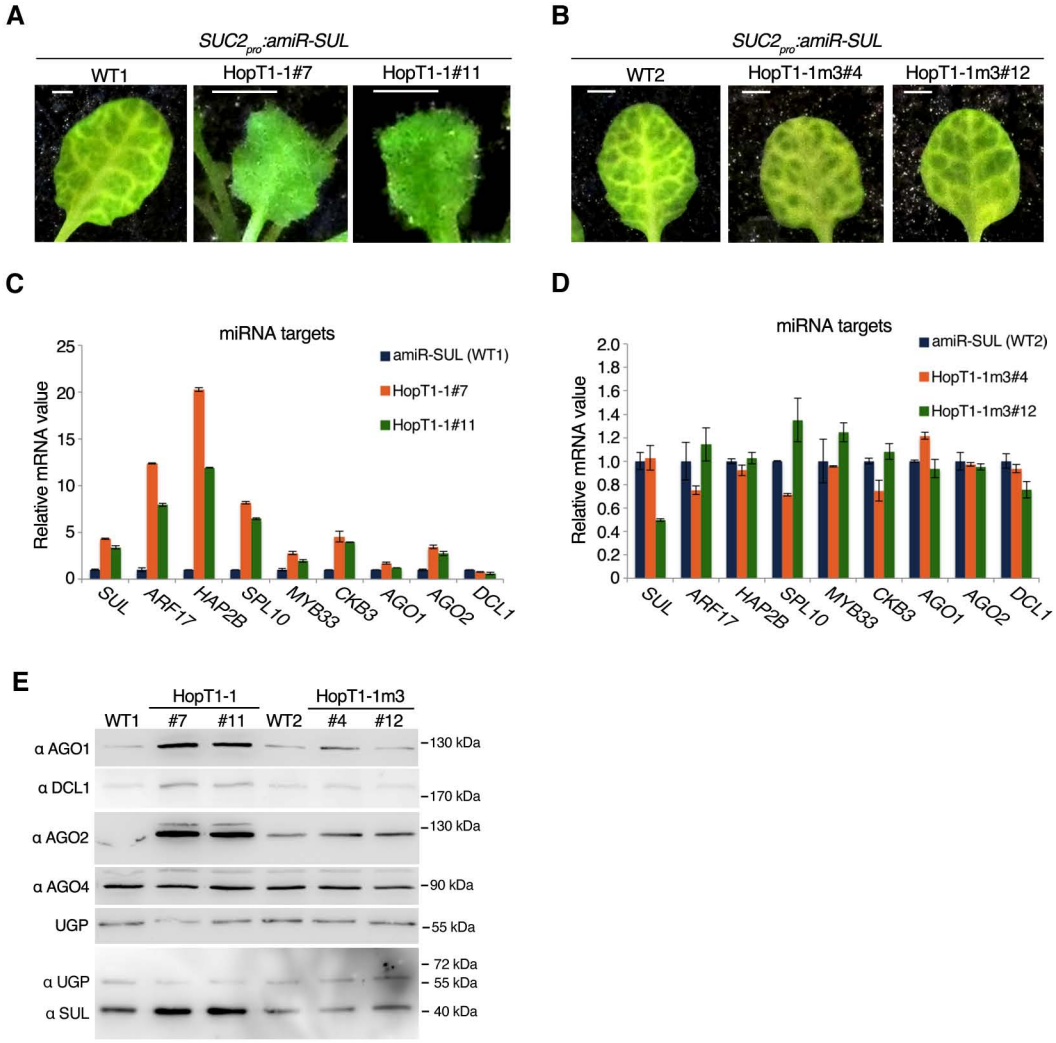

Figure 3. HopT1-1 suppresses AGO1-mediated miRNA function in a GW-dependent manner
(A) Representative pictures of a leaf of six-week-old *SUC2$_{pro}$:amiR-SUL* plants (WT1) along with independent T2 transgenic *SUC2$_{pro}$:amiR-SUL* plants constitutively expressing HopT1-1. White bar represents 0.5 cm. **(B)** Same as (A), but pictures of five-week-old *SUC2$_{pro}$:amiR-SUL* plants (WT2) along with independent T2 transgenic *SUC2$_{pro}$:amiR-SUL* plants constitutively expressing HopT1-1m3. White bar represents 0.5 cm. Plants were grown in parallel and in the same growth condition to the plants depicted in (A) but were collected one week before. For the molecular analysis, leaves from six plants were collected and pooled from HopT1-1 and HopT1-1m3 expressing transgenic lines along with WT1 and WT2, respectively. **(C)** Relative mRNA accumulation levels of *SUL* and multiple endogenous miRNA target transcripts in the HopT1-1 expressing transgenic lines in comparison to WT1 were monitored by RT-qPCR analysis. *Ubiquitin* was used as a control and the error bars represent the standard deviation from three technical replicates. **(D)** Same as (C) but using the HopT1-1m3 expressing transgenic lines in comparison to WT2. **(E)** Protein accumulation level of some endogenous miRNA targets AGO1, DCL1 and AGO2, was assessed by immunoblotting. Similarly, SUL protein accumulation level was also monitored. Protein accumulation level of AGO4 was used as an internal control, as this silencing factor is not targeted by any miRNA. UGP protein accumulation level was used as loading control.

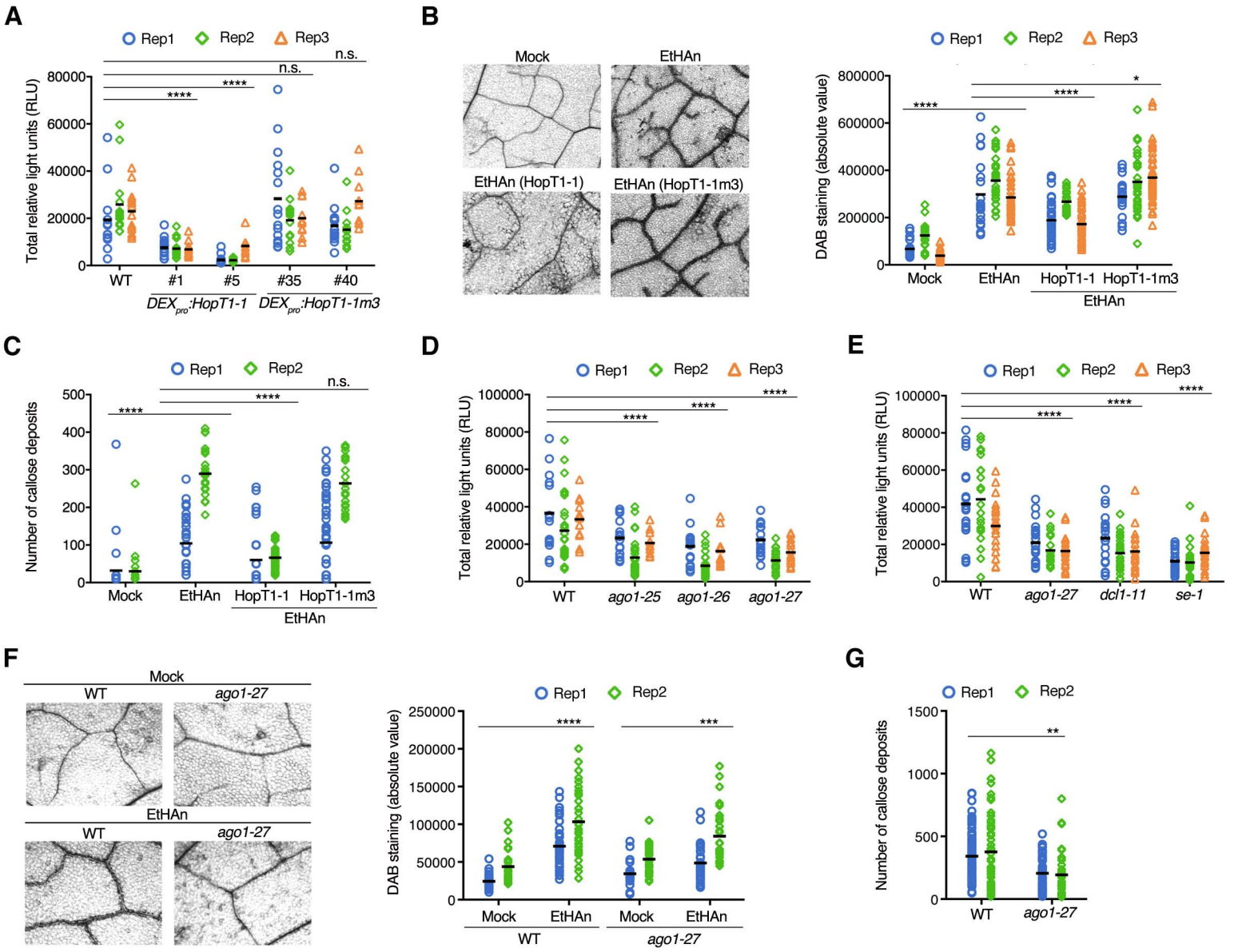

Figure 4. HopT1-1 dampens PTI in a GW-dependent manner and its presence mimics the impaired PTI responses observed in *ago1* mutants

(A) Flg22-induced ROS production assay was performed in leaf discs from DEX-treated samples. Five-week-old Col-0 Arabidopsis (WT) plants and T2 transgenic lines expressing Myc-HopT1-1 or Myc-HopT1-1m3 under the dexamethasone (DEX) inducible promoter (*DEX$_{pro}$:HopT1-1* and *DEX$_{pro}$:HopT1-1m3*, respectively) were sprayed every 24 hours for three consecutive days with 30 µM of DEX. For each condition, leaves from three plants were subsequently used to prepare leaf discs. Luminescence (Relative Light Unit; RLU) was measured over flg22-elicitated time-course for each technical replicate. Each dot represents the total amount of RLU produced during the flg22-elicitated time-course and the mean is represented as horizontal bar in the dot plot. Plants expressing Myc-HopT1-1 exhibit significant reduction in flg22-induced ROS production compared with WT plants or plants expressing Myc-HopT1-1m3. **(B)** Detection of H_2O_2 production in the leaves of WT plants 24 hours after infiltration with the EtHAn strain alone (EtHAn) or with EtHAn strain carrying a plasmid encoding for HopT1-1 or HopT1-1m3, respectively (left panel). Around 20-30 pictures were taken for each condition and leaves from three plants were treated to clear the chlorophyll pigments and were further incubated with DAB staining buffer to detect the presence of H_2O_2. In each condition, absolute value of DAB staining was quantified using ImageJ software and presented as a dot plot (right panel). **(C)** Presence of callose deposits was detected 7 hours after infiltration of WT plants with the EtHAn strains used in (B). For each condition, leaves from three plants were collected and stained with aniline blue to detect the presence of callose deposits. The amount of callose deposits was measured using ImageJ software and presented as a dot blot. **(D)** As in (A) but in WT and *ago1* mutant alleles, *ago1-25*, *ago1-26* and *ago1-27*. **(E)** As in (A) but in WT, *ago1-27*, *dcl1-11* and *se-1* mutants. **(F)** Same analysis as in (B) but in mock or in EtHAn-infiltrated plants on WT plants versus *ago1-27* mutant. **(G)** Same analysis as in (C) but in mock or in EtHAn-infiltrated plants on WT plants versus *ago1-27* mutant.

Note: For all the above experiments, statistical significance were assessed using the ANOVA test (n.s.: p-value>0.05; *: p-value<0.01; **: p-value<0.001; ***: p-value<0.0001; ****: p-value<0.00001). All the results shown in different panels of the figure were obtained in at least two or three independent experiments represented in the dot plots as Rep1, Rep2 and Rep3 respectively.

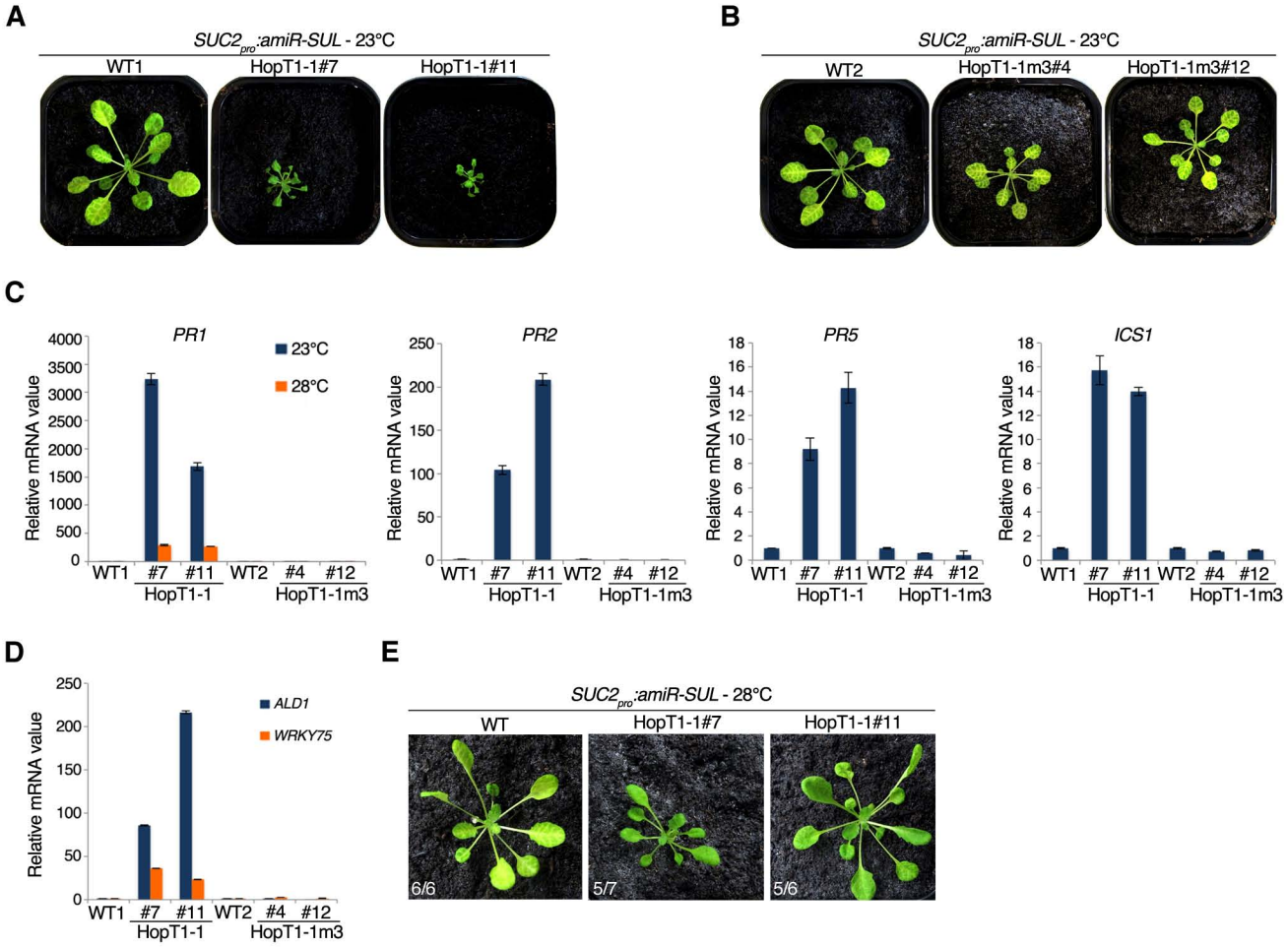

Figure 5. The BSR activity of HopT1-1 triggers a potent ETI response that is compromised at high temperature regime
(A) Representative pictures of six-week-old *SUC2$_{pro}$:amiR-SUL* plants (WT1) along with independent T2 transgenic *SUC2$_{pro}$:amiR-SUL* plants expressing HopT1-1. The HopT1-1 expressing plants shows dwarf phenotype as compared to WT1 plants when grown at 23°C. **(B)** Same as (A) but pictures of five-week-old *SUC2$_{pro}$:amiR-SUL* plants (WT2) along with independent T2 transgenic *SUC2$_{pro}$:amiR-SUL* plants expressing HopT1-1m3. No distinct phenotype was observed for these plants when compared to WT2. **(C)** Relative mRNA levels of *PR1* in HopT1-1 and HopT1-1m3 expressing plants compared with WT1 and WT2, respectively, was performed by RT-qPCR analysis. Similarly, relative mRNA levels of other SA-dependant markers like *PR2*, *PR5* and *ICS1* were also monitored. *Ubiquitin* was used as a control and the error bars represent the standard deviation from three technical repeats. Higher transcript levels were obtained for the plants expressing HopT1-1 as compared to WT and HopT1-1m3. **(D)** Same as in (C) but, relative mRNA accumulation level of cell death (*ALD1*) and senescence marker (*WRKY75*) was monitored. **(E)** Wild-type *SUC2$_{pro}$:amiR-SUL* plants and transgenic *SUC2$_{pro}$:amiR-SUL* plants expressing HopT1-1 were grown in parallel at 23°C and at 28°C. Representative pictures of the plants growing at 28°C are presented.

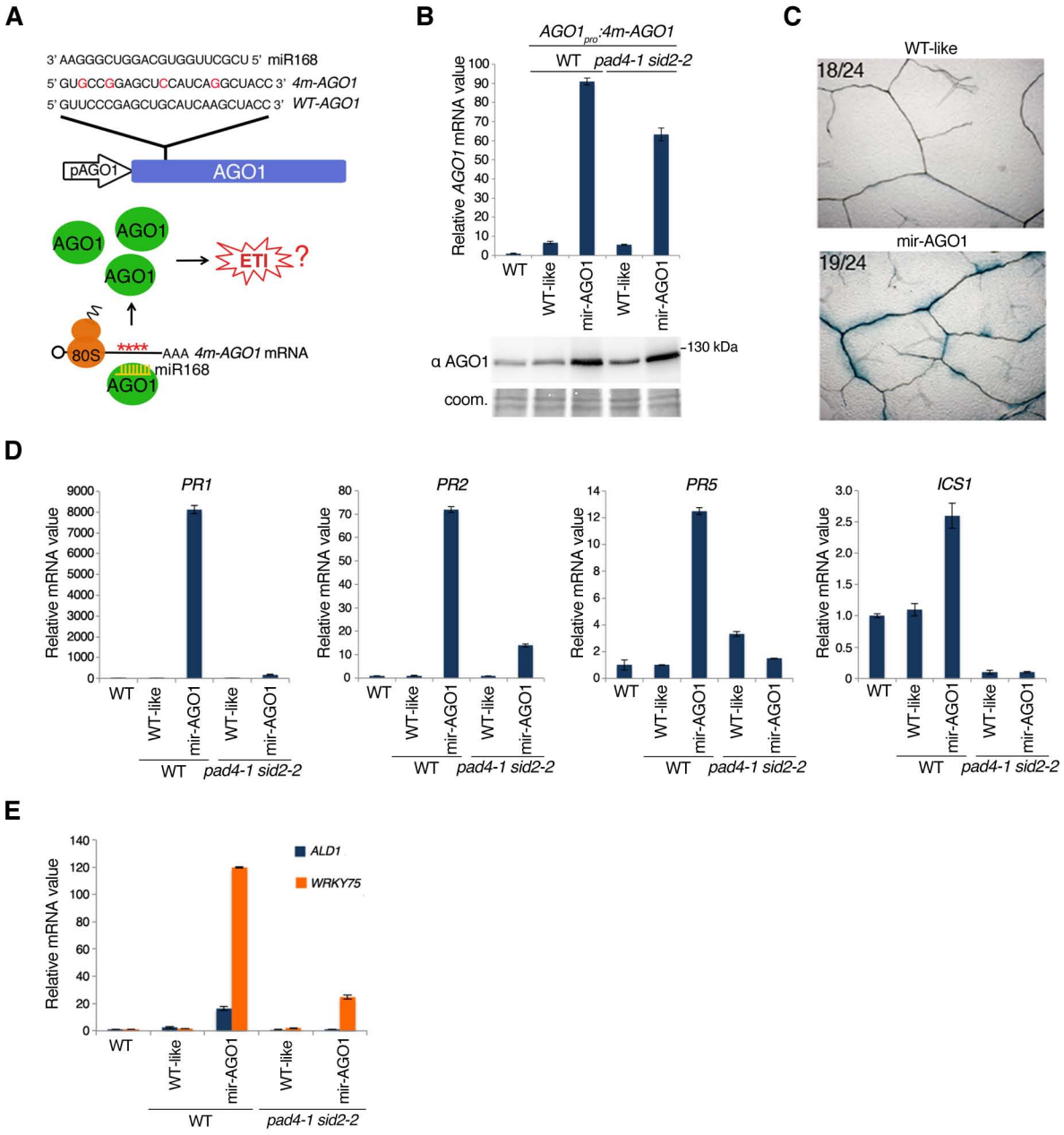

Figure 6. Stable expression of an AGO1 transgene that is refractory to miR168 is sufficient to trigger an ETI-like response
(A) Upper panel: Schematic representation of the *AGO1*$_{pro}$*:4m-AGO1* (*4m-AGO1*) transgene that is refractory to miR168 action under the control of the native AGO1 promoter. Four silent mutations (in red) were introduced (*4m-AGO1*) in the miR168 target site of AGO1. Bottom panel: Schematic representation of the hypothesis by which over-accumulation of the miR168-refractory version of AGO1 may trigger an ETI-like response. **(B)** *AGO1*$_{pro}$*:4m-AGO1* construct was transformed in WT plants or in *pad4-1 sid2-2* mutant. Primary transformants show a WT-like or a mir-AGO1 phenotype in both WT and *pad4-1 sid2-2* mutant. Leaves from a pool of six-week-old primary transformants exhibiting the same phenotype were collected for molecular analysis. Relative *AGO1* mRNA levels in WT plants or in *4m-AGO1* transgenic plants, was monitored by RT-qPCR analysis using *Ubiquitin* as control and the error bars represent the standard deviation from three technical repeats. Protein accumulation of AGO1 was assessed by immunoblotting. Coomassie staining was used as a loading control. **(C)** To detect the presence of cell death, trypan blue staining was performed on leaves of WT-like and mir-AGO1 plants. Representative pictures are depicted along with the number of pictures showing the same phenotype as compared to the total number of pictures taken. Plants with mir-AGO1 phenotype exhibit constitutive cell death within and around Arabidopsis leaf vasculature. **(D)** Relative mRNA level of *PR1*, *PR2*, *PR5* and *ICS1/SID2* mRNA was monitored byRT-qPCR analysis from the same samples used in (B). **(E)** Same as in (D) but *ALD1* and *WRKY75* mRNA levels were monitored. Note: All the results shown in the different panels of the figure were obtained in two independent experiments.

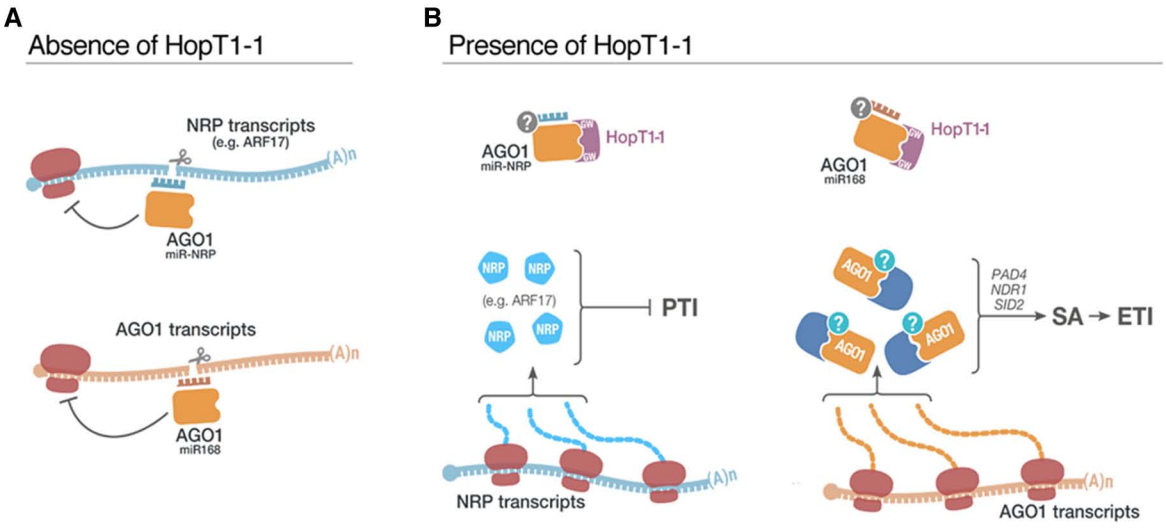

Figure 7. Hypothetical model for HopT1-1-induced molecular effects in host cells
(A) Representation of Negative Regulator of PTI (NRP)-, and *AGO1*- transcripts that are targeted by miRNAs in the absence of HopT1-1. MiRNA species that target NRP transcripts (in blue) and MiR168 species (in orange) are loaded in AGO1. **(B)** HopT1-1 interacts with AGO1 in a GW-dependent manner to suppress AGO1 silencing activity. In the model we propose possible mechanisms by which HopT1-1 might suppress PTI and trigger ETI. In the presence of HopT1-1, AGO1 is no longer able to trigger silencing of NRP mRNAs, which results in an enhanced production of NRPs, such as *ARF17* that can contribute to PTI suppression (left panel). Similarly, in the presence of HopT1-1, AGO1 is no longer able to silence its own transcript, which results in AGO1 protein hyper-accumulation. Perturbation of miR168-directed control of AGO1 homeostasis might be sensed by yet-unknown NLR proteins that are there to guard the integrity of AGO1 homeostasis. HopT1-1-induced disruption of AGO1 homeostasis results in a *PAD4*-/*NDR1*-/*SID2*-dependent immune response that culminates in SA-dependent signalling and ETI (right panel). Question marks depict hypothetical molecular effects that have not been experimentally validated. Indeed, we still do not know whether or not HopT1-1 could interfere with the loading of miRNAs in AGO1 or whether NLRs can directly bind to AGO1.